Master Thesis

im Rahmen des
Universitätslehrganges „Geographical Information Science & Systems“
(UNIGIS MSc) am Interfakultären Fachbereich für GeoInformatik (Z_GIS)
der Paris Lodron-Universität Salzburg

zum Thema

Estimation of grassland use intensity and mowing events

based on SAR coherence and Sentinel-2 MSI time series

vorgelegt von

Sandro Urf, BSc
104839, UNIGIS MSc Jahrgang 2017

Betreuer/in:
Prof. Dr. Stefan Lang

Zur Erlangung des Grades
„Master of Science (Geographical Information Science & Systems) – MSc(GIS)”

München, 31. Mai 2020

Acknowledgement

The present thesis was carried out at GAF AG, Munich, embedded in EcoLaSS-project. Above all, I would like to thank GAF AG and its team of the EcoLaSS-project for giving me the opportunity to write my master's thesis within a professional framework on such an exciting, valuable and future-oriented topic. Especially Fabian Berndt supported and motivated me with a lot of encouragement and always with helpful feedback, discussions and suggestions.

For the interesting and insightful GIS modules and the competent support during my studies, many thanks to the UNIGIS Team of the University of Salzburg.

Last but not least, I would like to thank all my family and friends for their support, assistance and patience during my studies. It would not have been possible without you.

Science Pledge

By my signature below, I certify that my thesis is entirely the result of my own work. I have cited all sources I have used in my thesis and I have always indicated their origin.

Sandro Urf

Munich, 5/31/2020

Content

List of Figures

List of Tables

Abbreviations

Abbreviation	Description
AOI	Area of Interest
ASC	Ascending
DEM	Digital Elevation Model
DESC	Descending
EAGF	European Agricultural Guarantee Fund
EC	European Commission
EcoLaSS	Evolution of Copernicus Land Services based on Sentinel data
EO	Earth Observation
EU	European Union
EVI	Enhanced Vegetation Index
EVI 2	Enhanced Vegetation Index 2
GNDVI	Green Normalized Difference Vegetation Index
GRD	Ground Range Detected
HNV	High Nature Value
HR	High Resolution
HRL	High Resolution Layer
IACS	Integrated Administration and Control System
InSAR	Synthetic Aperture RADAR Interferometry
INVEKOS	Integriertes Verwaltungs- und Kontrollsystem
IR	Infrared
IRECI	Inverted Red Edge Chlorophyll Index
LAI	Leaf Area Index
LC	Land Cover
LCI	Leaf Chlorophyll Index
LOI	Location of Interest
LU	Land Use
LUCAS	Land Use and Coverage Frame Survey
MS(I)	Multispectral (Instrument)
NDVI	Normalized Difference Vegetation Index
NDWI	Normalized Difference Water Index
OA	Overall Accuracy
PA	Producer´s Accuracy
RADAR	Radio Detection and Ranging
RF	Random Forest
S-1	Sentinel-1
S-2	Sentinel-2
S2REP	Sentinel 2 Red Edge Position
SAR	Synthetic Aperture RADAR
SAVI	Soil Adjusted Vegetation Index

SD	Standard Deviation
SLC	Single Look Complex
SRTM	Shuttle Radar Topography Mission
SVM	Support Vector Machine
UA	User´s Accuracy
UAV	Unmanned Aerial Vehicle
UVN	Ultraviolet Visible Near-infrared
UVNS	Ultraviolet Visible Near-Infrared Shortwave
VHR	Very High Resolution
VI	Vegetation Index

1. Introduction

Grassland ecosystems are of the highest importance in terms of ecological factors such as floral and faunal biodiversity and the global carbon sink, but also regarding economic considerations like their major role in feed source for livestock. With 31.5%, or approximately 42 million square kilometres, grassland claims the biggest share among all land cover classes of the world (tree covered areas: 27.7%; bare soil: 15.2; cropland: 12.6%; without Antarctica). In a manner of speaking about Europe, 8% of the total area is declared as grassland and about 35% of the agricultural area can be assigned to various types of grassland (ALI et al. 2016: 1ff.; ISSELSTEIN et al. 2015: 8f.; LATHAM and CUMANI 2014: 23; SCURLOCK and HALL 1998).

Overgrazing, agricultural intensification and an increasing urbanization are endangering these valuable habitats and require state monitoring as well as regular monitoring of changes and their development. Special challenges for grassland mapping are, in addition to the different types of use, regional and local influences such as topographic circumstances, anthropogenic impact and climatic influences like dry periods (ALI et al. 2016; ISSELSTEIN et al. 2015; SCURLOCK and HALL 1998).

In terms of usage for monitoring and analyzations of grasslands as a fundamental land cover, remote sensing techniques, including aerial photography, satellite-based systems and radar sensors, developed to an essential instrument over the past 30 years. With the evolution of sensors over time, from moderate over high to very high resolution, also the appropriation of their data and fields of applications have developed. On a global to local scale these applications and methods include classic land cover/use classification, change detection and monitoring, production evaluation, grazing management assessment up to predictions of grassland herbage yields and carrying capacity. Therefore, various remote sensing techniques take advantage of the multi spectral sensors ability to process data of several bands (wavelengths) along the electromagnetic spectrum. Regarding the analysis of grassland, and vegetation in general, especially wavelengths in near infrared and red ranges are relevant due their capability of spectral response to chlorophyll activity. This characteristic is particularly used for the calculation of (vegetation) indices like the normal difference vegetation index (NDVI) (NAN 2001; TUELLER 1989).

Besides optical remote sensed data, several approaches to estimate and analyze characteristics of grassland include the usage of radar derived data. Especially for the implementation of land cover products, a combination of optical and radar sensors has developed to a common procedure regarding compensating disadvantages of each sensor, resulting in additional value for further investigations and derivations regarding grassland applications (DUSSEUX et al. 2014; HONG et al. 2014; NICULESCU et al. 2018b).

Within EU´s earth observation program, managed and coordinated by the European Commission (EC), Copernicus Services provide environmental information in multiple thematic departments including land, marine, atmosphere and emergency management largely based on remote sensed satellite data. In the sector of Copernicus Land Services, the EcoLaSS project (Evolution of Copernicus Land Services based on Sentinel data) aims to develop, enhance and implement methods, processes and prototypes regarding land cover (LC) and land use (LU) products using dense Sentinel-satellite time series including synthetic aperture radar (SAR) and multispectral optical data.

Within this context, EcoLaSS-products cover LC/LU prototypes in thematic areas of agriculture, forest, imperviousness and grassland with key objectives of methodological development of innovative processes and their embedding in an operationalization framework (DLR 2020; EUROPEAN COMMISSION 2019; JOANNEUM RESEARCH 2019: 6f.).
This thesis is written as part of EcoLaSS-project, aiming for theoretical and practical input for an improved permanent grassland identification and its assessment of grassland management intensity in ongoing and future Land Cover and Land Use products.

2. Theoretical Background

This chapter provides an overview of technical and theoretical principles and terms regarding satellite based remote sensing concepts, both optical and SAR-derived, pertinent to the thesis´ purpose. Furthermore, availed classifiers and the approach of land cover classifications are presented and outlined.

2.1. Remote Sensing and Space Imaging

The concept of remote sensing includes all processes of obtaining information about an area or objective without direct contact of the measuring device and the investigated object. Referring to the Canadian Centre of Remote Sensing it defined as

> "(…) the science (and to some extent, art) of acquiring information about the Earth's surface without actually being in contact with it. This is done by sensing and recording reflected or emitted energy and processing, analyzing, and applying that information." (CCRS n.d.: 5)

The sensor or measuring device is in general not platform-bound and can be mounted on a plane, satellite or a terrestrial stand. First attempts of space imaging took place with the launches of the first satellites during cold war's space race in the 1950s and 1960s. Primary use was given by military interests on sides of the US and former UDSSR. For the civil sector, satellite-based products got available in the 1960s with manned space programs and the first meteorological satellites (CRACKNELL 2018: 8393ff.; LILLESAND et al. 2008: 1ff; 397ff.).

A common differentiation of remote sensing systems takes place in active and passive systems. Regarding their capability of sending and/or emitting radiation, a sensor or a system is assigned to one of these main groups. For both fractions, information is obtained along the electromagnetic spectrum. For remote sensing sensors in general, specific regions of the spectrum, ranging from ultraviolet to microwave, are particularly useful and, as shown in Figure 1, visible radiation (0.4-0.7µm) represents just a small range along the electromagnetic spectrum. Therefore, with remote sensing sensors it is possible to obtain additional information not detectable by the human eye. Such information can be collected e.g. in wavelengths of 0.7-1µm, respectively the infrared region of the electromagnetic spectrum. For example, due to high reflectance of chlorophyll at IR-wavelengths, this range is especially used for applications with the need of information about vegetation. On the other hand, longest wavelengths used in remote sensing are microwaves with 1mm up to metres with applications within fields of e.g. soil moisture estimation, snow studies and flood mapping (CALLA 1990: 343f.; CCRS n.d.: 9ff.; KHORRAM et al. 2016: 11ff.).

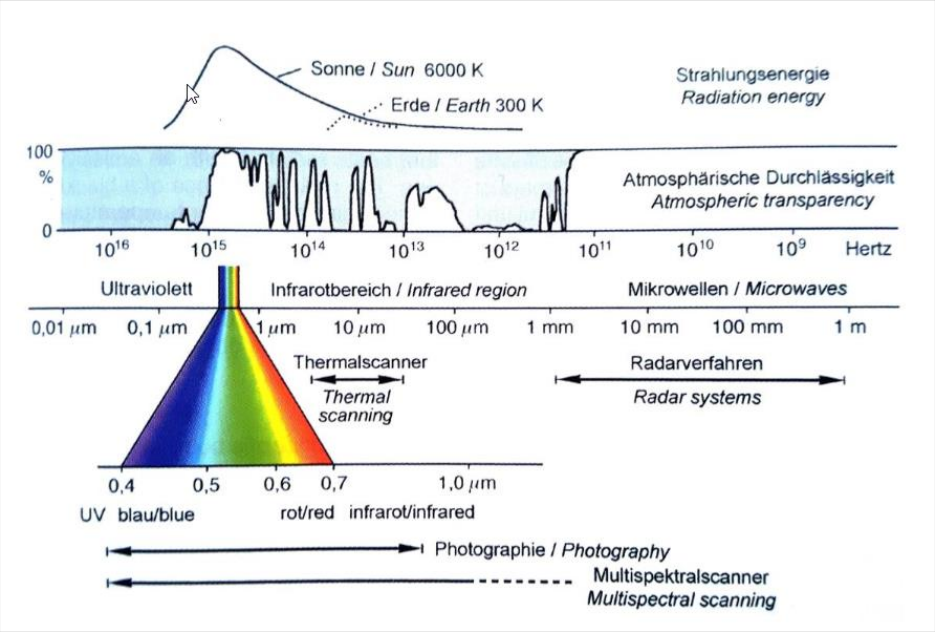

Figure 1: The electromagnetic spectrum (ALBERTZ and WIGGENHAGEN 2009).

Referring to KHORRAM (2016: 21ff.) and LEVIN (1999: 38ff.) further differentiation of satellite based remote sensed data can be obtained with the following characteristics:

a. Spatial resolution: Referring to the resolution ground-truth represented in one pixel of the recorded image; e.g. one pixel represents 10x10m.
b. Spectral resolution: Range on the electromagnetic spectrum, which can be recorded by the sensor; e.g. panchromatic, multispectral, hyperspectral.
c. Temporal resolution: Timespan of the satellite to revisit the same location on earth's surface for the image; e.g. Landsat-8: 16 days; Sentinel 2A/B: 5 days.
d. Radiometric resolution: Dynamic range of the sensors sensitivity regarding the electromagnetic reflectance specified in bits providing detailed information (grayscale); e.g. 8-bit, 12-bit, 16-bit.

2.1.1. Optical

Satellite systems with sensors operating in a wavelength range of 0.3-1.4µm are categorized as optical sensors. Besides the wavelengths of visible light, UV (ultra-violet), near- and mid IR (infrared) wavelengths are included (Figure 1). Optical sensors measure radiation emitted on a natural way, mostly by the sun, and reflected from the earth´s surface. Due to their dependency of not-self-emitted radiation, optical sensors are generally also categorized within the group of passive remote sensing systems (CCRS n.d.: 19; KHORRAM et al. 2016: 13f; LILLESAND et al. 2008: 392ff.).
As outlined, optical sensors have the ability to process the reflected radiation from a given surface. Each surface shows its individual amount of reflected radiation at specific wavelengths, resulting in a spectral signature or spectral response curves for each surface (Figure 2). Especially the high response/peak of vegetation at near-infrared wavelengths is a characteristic strength of optical remote sensed data and is reconsidered in various discussed studies (s. chapter 1 and chapter 3).

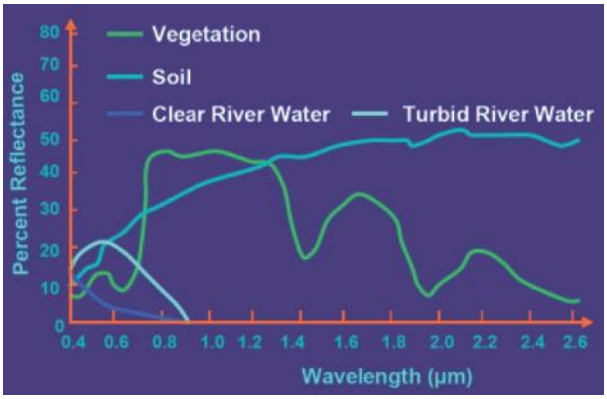

Figure 2: Examples for spectral signatures (KHORRAM et al. 2016: 70).

2.1.2. RADAR/SAR

RADAR/SAR (radio detection and ranging/synthetic aperture radar) is categorized as an active remote sensing method due to the capability of emitting electromagnetic pulses by itself. SAR itself is a specific form of RADAR technology, using the flight path of the satellite/aircraft to simulate an oversized antenna capable to generate high resolution imagery without the physical necessity of an antenna with such dimensions by increasing the azimuth resolution at minimum altitude. Consisting of a transmitter, a receiver and an antenna, its essential purpose is a distance measuring device. Radiation is sent threw an antenna at regular intervals or pulses, reflected on earth's surface and a sensor records the intensity and operational time of returned radiation respectively the backscattered echo (CCRS n.d.: 71; KHORRAM et al. 2016: 36; WOLFF n.d.).

An essential advantage of RADAR and SAR-imagery in comparison to optical data is the independency of day/night cycle and its capability to be resistant in terms of cloud occurrence or other atmospheric scattering. Compared to visible and near-infrared region of the electromagnetic spectrum, the microwave region is considerable larger with wavelengths ranging from sub-centimeters to meters. Depending on the signal´s wavelength, the RADAR/SAR radiation interacts in different ways with the investigated object resulting in versatile applications for different microwave bands. The main fields of those applications are in vegetational, land monitoring and maritime themes and topics. The higher the wavelength, the deeper its ability to penetrate the given surface; e.g. a shortwave X-band (~3cm wavelength) interacts mainly with vegetation´s canopy, while a long wavelength L-band (15-30cm) is able to interact with tree trunks and underneath lying soil (Table 1) (CCRS n.d.: 71, 96f; KHORRAM et al. 2016: 36,148f.; WOLFF n.d.).

Table 1: RADAR bands and wavelengths (MOREIRA et al. 2013: 7)

Band	Wavelength (cm)
Ka	0.75 – 1.2
Ku	1.7 – 2.5
X	2.5 – 4
C	4 – 8
S	8 – 15
L	15 – 30
P	60 - 120

From the sensor recorded reflected radiation is summarized in the process of backscattering. Radar backscatter is mainly affected by the incident angle and roughness of the surface of observed area or object. Usually, in radar images a higher amount of backscatter is symbolized with brighter tones than low backscatter. As shown in Figure 3, a rough surface (a), like vegetation, scatters the energy mostly equally in all directions (diffusely) leading to significant backscattering. A smooth surface (b) will reflect specular, leading to a small amount of energy returned to the sensor, respectively a low backscatter. Corner reflection (c) occurs especially in urbanized areas and is a typical characteristic of buildings and other man-made-structures but can also be seen in mountainous areas with rock and cliff formations. Due to the 'double bounce' and nearly right angles, most of the energy is directly reflected to the sensor leading to a very bright occurrence of the observed object. (CCRS n.d.: 106ff; LILLESAND et al. 2008: 159ff).

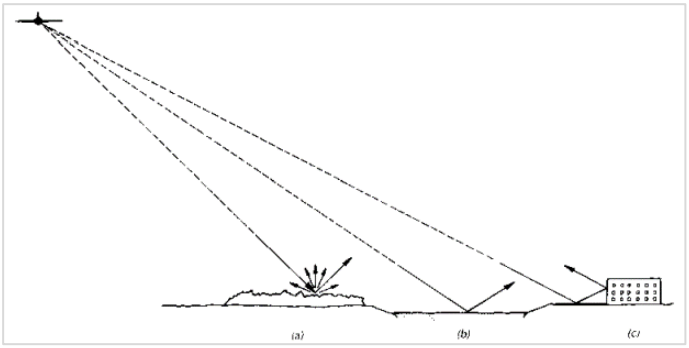

Figure 3: Radar reflections. a) diffusely; b) specular; c) corner (LILLESAND et al. 2008: 660).

SAR´s backscattered information is also affected by the sensor's polarization. Referring to the orientation of the emitted radiation´s electric field, RADAR/SAR sensors can provide multiple polarization modes. This can be a single polarization (vertical or horizontal) or dual polarization depending on the sensors ability to send and receive the microwave radiation, following in these possible combinations of polarizations (a schematic illustration is provided in Figure 4):

- HH: sending in horizontal plane and receiving in horizontal plane
- HV: sending in horizontal plane and receiving in vertical plane
- VV: sending in vertical plane and receiving in vertical plane
- VH: sending in vertical plane and receiving in horizontal plane

Furthermore, radar systems can be categorized in their capability to transmit and receive radiation of specific polarizations leading to following sensor characteristics:

- single polarized: HH or VV (or possibly HV or VH)
- dual polarized: HH and HV, VV and VH, or HH and VV
- alternating polarization: HH and HV, alternating with VV and VH
- polarimetric: HH, VV, HV, and VH

Depending on the transmitted and received radiation´s polarization, the interaction with the surface, respectively the backscatter, is affected, leading to slightly different information depending on chosen polarization. This characteristic can help to improve the delimitation and identification of observed features (CCRS n.d.: 97f, 115ff; LILLESAND et al. 2008: 664 f.; VOORMANSIK et al. 2016; VOORMANSIK et al. 2013).

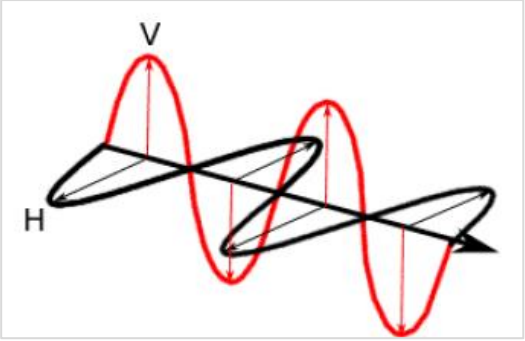

Figure 4: Scheme of horizontal and vertical polarization (CCRS n.d.: 117).

In comparison to optical sensors and due to their physical characteristics, SAR-sensors make use of the RADAR/SAR-typical side-looking acquisition. Figure 5 shows the scheme of a side-looking system. (A) represents the incident angle between the radar beam and the ground surface which increases by moving along (D) the ground range distance. (B) refers to the look angle. In near range, the viewing geometry is steeper than in far range, where it is considered shallower. The slant range distance (C) is defined by the distance (line of sight) between the sensor and each captured target located on the ground. Because of this characteristics, including side-looking acquisition, the dynamic slant range and incident angles, the viewing geometry and spatial resolution of SAR-derived products are different from optical products and contain compressed and stretched areas (Figure 6) with need to be processed depending on considered application (CCRS n.d.: 102f.; LEVIN 1999: 136f.).

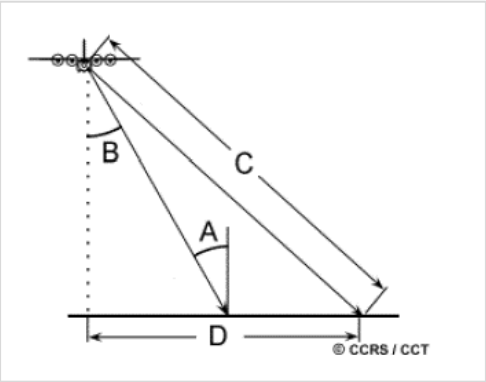

Figure 5: Scheme of side-looking SAR acquisition (CCRS n.d.: 100)

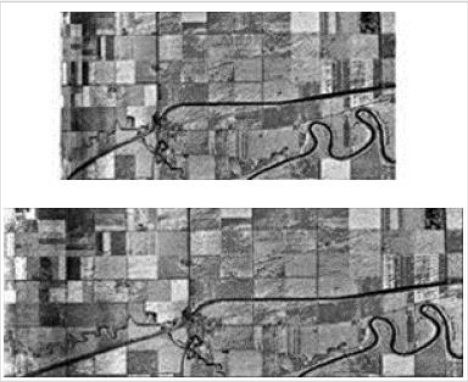

Figure 6: Comparison of slant-range geometry (top) and ground-range geometry (bottom) (CCRS n.d.: 102).

Depending on further usage of the SAR image, GRD (Ground Range Detected) and SLC (Single Look Complex) products are available. GRD-products consist of focused, multi-looked (speckle-filtering) and projected SAR-data. Delivered pixel-information contains amplitude-values; phase information is not available for GRD-products. Due projection and algorithm application, the resulting image is available in square resolution to further usage. SLC-products consist of focused, geo-referenced SAR-data contributed in slant-range geometry (line of sight from radar to each point of reflectance). Phase information is preserved in SLC-products (EUROPEAN SPACE AGENCY ESA 2000a).

Furthermore SAR-products can show additional distortions leading to relief displacements caused by its mentioned characteristics. These are foreshortening, layover and shadow effects.

Foreshortening

Relief displacement of foreshortening occurs, when the radar beam records a tall feature tilted towards the sensor. Because of the slant-range distance, the beam reaches the bottom of the object before the object´s top. Figure 7 shows foreshortening displacement of slope A to B. Slope A-B will be represented compressed and therefore incorrectly. As shown, the foreshortening-effect depends on the angle of the hillside as well as the incidence angle of the radar beam (CCRS n.d.: 102f; LEVIN 1999: 136f.)

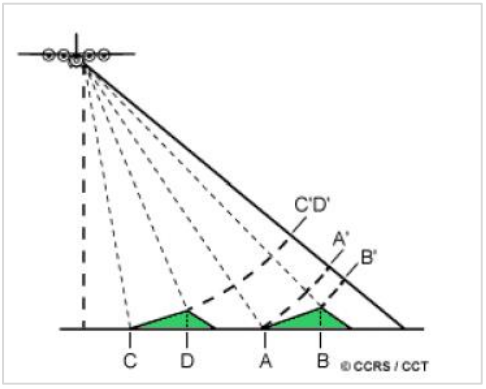

Figure 7: Illustration of foreshortening (CCRS n.d.: 103).

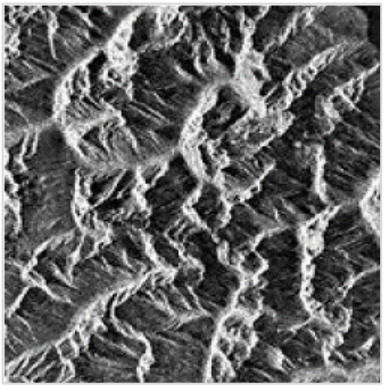

Figure 8: Radar image with foreshortening (bright features) (LEVIN 1999: 137).

Layover

Layover-effect occurs when the radar beam reaches the top a high object before it reaches its bottom so the signal from the top is recorded before the base reflection. The top of the feature will be displaced towards the sensor and shows a displacement from its ground position. Figure 9 shows an illustration of the layover-effect. The top, B, falls over the base, A, towards the sensor resulting in relief displacement as shown in the radar image in Figure 10 (CCRS n.d.: 104; LEVIN 1999: 137).

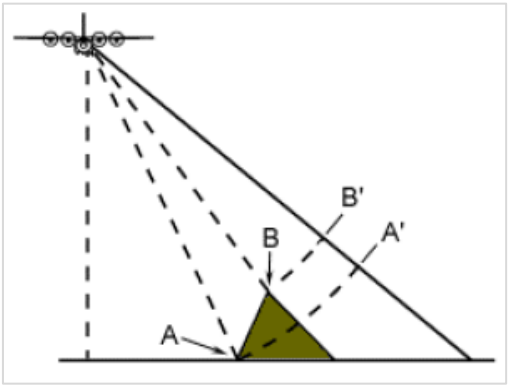

Figure 9: Illustration of layover(CCRS n.d.: 104).

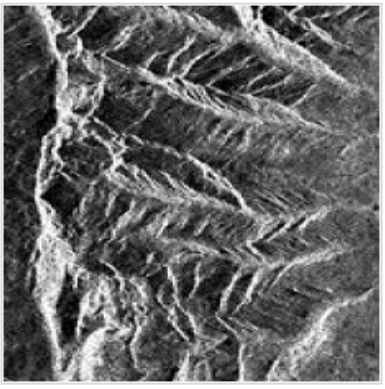

Figure 10: Radar image with layover (LEVIN 1999: 137).

Shadow effects

Both discussed effects, foreshortening and layover, can generate radar shadow. This occurs when the radar beam is not able to illuminate a surface and therefore a reflectance of the surface is not given. An illustration of shadow effects and its dependency on the incident angle and the height of the recorded object is shown in Figure 11. A radar image with given effect is shown in Figure 12. In this example, with illumination from the left, shadow effects appear as black in the mountainous areas.

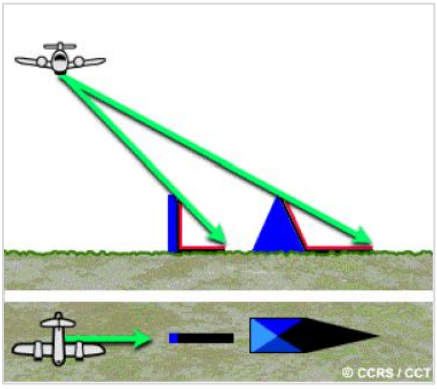

Figure 11: Illustration of shadow effect (CCRS n.d.: 105).

Figure 12: Radar image with shadow effect (LEVIN 1999: 138).

SAR Interferometry

Every SAR signal incorporates amplitude and phase information, meaning the strength of the radar response and the fraction of one wave circle (single SAR wavelength). The idea of SAR Interferometry (InSAR) is the phase comparison of two SLC radar images acquired from a slightly different position or at a different time. This is obtained by a slight offset of the waves resulting in a phase difference after coregistration. Since every pixel contains range information, small differences in scales up to of millimeters can be detected. Given this capability, applications using InSAR include geophysical topics like glacier movements, ground deformations, seismic deformations and volcanic activities. Figure 13 shows an example of an interferogram used for ground deformation. In a further step, the correlation between several acquisitions can be calculated resulting in their coherence. With coherence calculations, land cover classification and change detection can be obtained. Due to correlation calculation, coherence estimation also allows to detect characterizations of vertical structures from volume scatterers like vegetation. Figure 14 shows a cultivated parcel with low coherence (left) and high coherence (right) indicating land management activities (CCRS n.d.: 114ff.; EUROPEAN SPACE AGENCY ESA 2000b; LEVIN 1999: 145ff.; MOREIRA et al. 2013: 6ff; 19ff.).

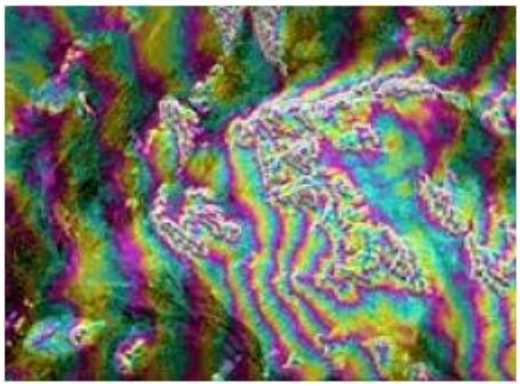

Figure 13: Example of interferogram (LEVIN 1999: 146).

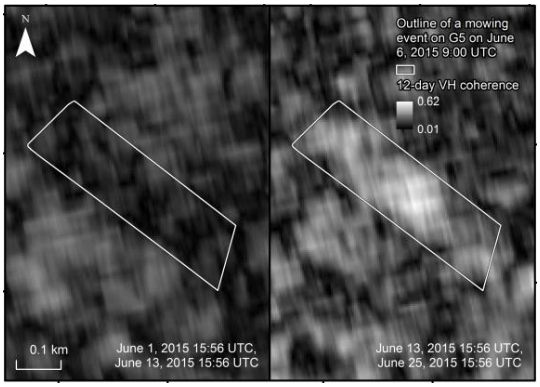

Figure 14: Example of coherence; left: low coherence; right: high coherence (TAMM et al. 2016: 10).

2.2. Sentinel Satellite Program

Initiated by the European Space Agency (ESA), Sentinel satellite programs include various earth observation missions within European earth observation program Copernicus. In collaboration of the European Environment Agency (EEA), ESA and EU-countries, the aim of Copernicus is to establish an observation infrastructure containing satellites and in situ sensors providing information related to environmental topics e.g. atmospheric-, marine- and land observation, climate change and issues regarding security and emergency response (EUROPEAN COMMISSION 2016; EUROPEAN SPACE AGENCY ESA 2000c).

The Sentinel satellite program consists of 6 missions in total (Sentinel 1, 2, 3, 4, 5, 5P), based on two satellites per mission. Each mission and sensor is defined with a specific purpose and sensor characteristic (EUROPEAN SPACE AGENCY ESA 2000c).

An overview of the entire Sentinel-mission is shown in Table 2. Regarding research undertaken in this thesis (chapter 4) and used data (chapter 5.1), the focus is set to Sentinel-1 and Sentinel-2 sensors, which are further discussed.

Table 2: Sentinel Missions; Overview (EUROPEAN SPACE AGENCY ESA 2000c; EUROPEAN SPACE AGENCY ESA 2000d; EUROPEAN SPACE AGENCY ESA 2000e).

Mission	Characteristics/Application	Launch
Sentinel-1	- RADAR (SAR) imaging sensor - Polar orbiting - land and oceanic services	S-1A: 2014 S-1B: 2016
Sentinel-2	- MSHR optical imaging sensor - Polar orbiting - land services (monitoring)	S-2A: 2015 S-2B: 2017
Sentinel-3	- Multi-sensor mission - marine observation (sea surface topography, sea and land surface temperature)	S-3A: 2016 S-3B: 2018
Sentinel-4	- UVN-sensor on Meteosat-satellite - geostationary - atmosphere / air quality monitoring	Scheduled 2021
Sentinel-5	- UVNS-sensor on MetOp-satellite - polar orbiting - atmosphere / air quality monitoring	Scheduled 2021
Sentinel-5P	- UVNS-sensor on MetOp-satellite - polar orbiting - atmosphere / air quality monitoring	2017

2.2.1. Sentinel-1

Sentinel 1 mission consists of a pair of satellites operating with a C-band synthetic aperture radar imaging sensor (wavelength 3,75 – 7,5cm) with the purpose of land and ocean monitoring.

The constellation of Sentinel-1A and Sentinel-1B operates in four acquisition modes (Figure 15), namely

- Stripmap (SM): 80km swath, one of six beams used;
- Interferometric Wide swath (IW): main operational mode, 250km swath, TOPSAR-technique: 3 sub-swaths with a series of bursts (Figure 16);
- Extra-Wide swath (EW): 410km swath, TOPSAR-technique: 5 sub-swaths;
- Wave (WV)

(EUROPEAN SPACE AGENCY ESA 2000f)

Modes SM, IW and EW are available in single (HH or VV) dual polarization (HH+HV or VV+VH) while WV mode is delivered with single polarization (HH or VV) only. For each mode, products are deliverable at three levels of processing – level 0, level 1 and level 2.

- Level-0: L-0-Raw data contains compressed, unprocessed SAR imagery. All advanced products are based on L-0 SAR data;
- Level-1: Obtained from L-0-products by pre-processing, doppler centroid estimation (polynomial fitting) and focusing. Products of L-1-processing are SLC or GRD-products;
- Level-2: Derived from Level-1 and used for applications regarding information about wind, wave and currents.

(CCRS n.d.: 96; EUROPEAN SPACE AGENCY ESA 2000f).

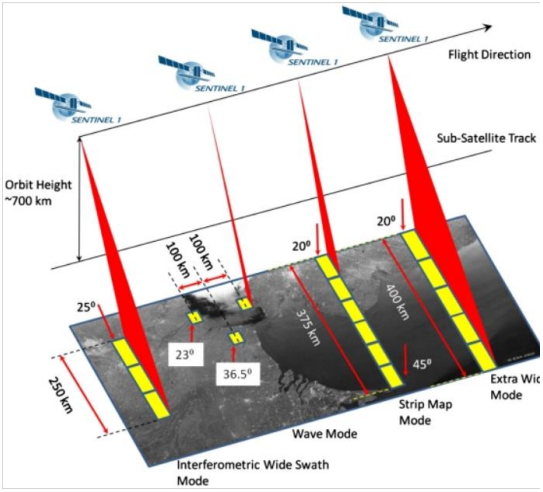

Figure 15: Sentinel 1 acquisition modes (EUROPEAN SPACE AGENCY ESA 2000f).

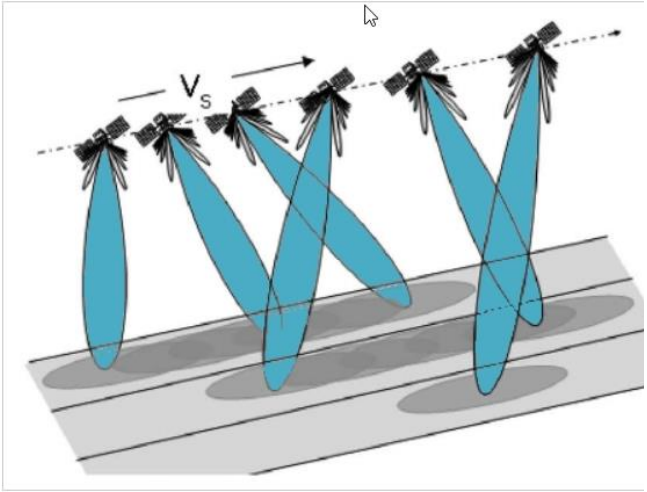

Figure 16: Sentinel 1 TOPSAR-technique (EUROPEAN SPACE AGENCY ESA 2000f).

2.2.2. Sentinel-2

Within the Copernicus program, Sentinel-2 is a pair of satellites equipped with a wide-swath, high resolution multi spectral instrument (MSI) with its purpose of earth observation. With the pair of Sentinel-2A and Sentinel-2B, a temporal resolution of five days can be achieved. Using one of the satellites, the timespan is expanded to a revisiting time of 10 days. Sentinel-2-MSI products are delivered in 100x100km tiles and are available without limitations at processing levels 1C and 2A. Processing level 1C (L1C) includes radiometric and geometric corrections with ortho-rectification

and spatial registration on a global reference system, while level 2A (L2A) is provided with specifications of L1C including an additional atmospheric correction and scene classification (EUROPEAN SPACE AGENCY ESA 2000g; EUROPEAN SPACE AGENCY ESA 2000h).
Table 3 gives an overview of the spectral bands, wavelengths and spatial resolution of Sentinel-2A and 2B sensor. Bands with the highest spatial resolution of 10 metres are assigned to visible wavelengths blue (band 2), green (band 3), red (band 4) and near-infrared wavelength (NIR) with band 8. Bands with 20 metre resolution are located in VNIR and SWIR-domains and are especially used in vegetation-, snow-, ice – and cloud detection, while bands with resolution of 60m are mainly used for atmospheric corrections (EUROPEAN SPACE AGENCY ESA 2000i).

Table 3: Sentinel 2 A/B Spectral Bands (EUROPEAN SPACE AGENCY ESA 2000g).

Spectral Band	Center Wavelength (nm)	Spatial Resolution (m)
Band 1	443	60
Band 2	490	10
Band 3	560	10
Band 4	665	10
Band 5	705	20
Band 6	740	20
Band 7	783	20
Band 8	842	10
Band 8a	865	20
Band 9	945	60
Band 10	1380	60
Band 11	1610	20
Band 12	2910	20

2.3. Land Cover Classification

With the launch of various satellite programs, equipped with specific sensors for monitoring purposes, new approaches for land cover mapping with precise results on a regularly basis have been allowed. Especially models on a global, continental and regional scale benefit from advantages of satellite and/or airborne based remote sensed data. Traditional methods of land cover/usage mapping have been based on field surveys, which are, in comparison to new methods, uneconomical and time-consuming with much higher resource input (ARORA 2010).
Within the process of remote sensing derived digital image classification techniques, principles include an assignment of each pixel to a defined class based on given values of a pixel, e.g. reflectance of specific wavelengths. Pixel based classification models can be differentiated based on their training process in supervised and unsupervised classifications. For a supervised classification, manual input in form of sample data or thresholds for desired classes are required. For the further classification process, characteristics of samples are crucial and have to be well chosen. Examples for supervised classifiers are Minimum Distance, Maximum Likelihood or Support Vector Machines classifiers. On the other hand, the unsupervised classification, there is no need for direct

human interaction. The classes depend solely on statistical clustering in the given feature space e.g. at K-means-clustering or ISODATA classifier (ARORA 2010; LILLESAND et al. 2008).

2.3.1. Random Forest

In the field of remote sensing, random forest is a well-established classifier for not only land cover classification. Numerous studies show its fields of application in data classifications of multispectral, LiDAR, thermal, radar, hyperspectral and multi-source data. Random forest is a supervised ensemble classifier, using predictions. As a combination of tree classifiers, each tree is generated by drawing a subset of training samples. Then, each classifier is trained on a random set of training samples. The process of implying a classification defined by a random subset of samples is called bagging. Its counterpart, using iterations over the whole sample ensemble, is called boosting. Approximately two thirds of the samples are used for the classification respectively to train the trees. Random forest uses the remaining third of samples for a cross-validation to measure the quality, respectively accuracy, of the model. Compared to other classification methods, random forest performs better and faster in most cases with multidimensional (hyperspectral) and multisource data than other classifiers (BELGIU and DRĂGUŢ 2016; PAL 2003; TSO and MATHER 2009: 215f.).

2.3.2. Support Vector Machine

Support Vector Machine (SVM) is a supervised statistical classification method. The idea of SVM is the separation of the input data in several predefined classes by constructing a hyperplane as a decision boundary. In its original form, used as a linear binary classifier, the hyperplane is set as the maximum margin between the classes respectively the sum of the distances from the closest points of each class to the hyperplane. The closest points of each class to the hyperplane define the margin and are therefore called 'support vectors' (Figure 17). For multi-class classifications, various adaptions of SVM have been introduced and show, as well as the original linear binary SVM, better results regarding performance than other established classification methods like maximum likelihood classifier (MOUNTRAKIS et al. 2011; PAL 2003: 218f.; TSO and MATHER 2009: 125).

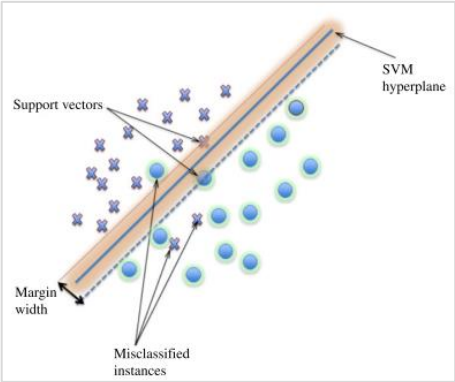

Figure 17: Illustration of SVM (MOUNTRAKIS et al. 2011: 248).

2.3.3. *Accuracy Assessment*

As a method to validate the results of a completed (landcover) classification, a well-established approach is the usage of confusions matrices. Especially for remotely sensed derived classification results this simple yet efficient technique is widespread and often used for accuracy assessment. An example of such table including a confusion matrix is shown in Figure 18. To obtain a confusion matrix, classified data is compared to ground truth, respectively reference data, resulting in a percentage value of correctly classified data. This is derived by summarizing the values of the major diagonal, expressed by classified pixels which are also assigned to the given class in the reference data, divided by the total numbers of classified pixels. Showing the general agreement between two datasets, the result is also named overall accuracy. For an in-depth analysis of the classification, each individual class can be evaluated by dividing the correctly classified pixels in the given category by either the total pixels of the congruent column or row. Results of this calculations lead either to producer´s accuracy (column) or user´s accuracy (row). Computing producer´s accuracy gives information about the probability of reference pixels being classified correctly, respectively an omission error´s determination. In another way, user´s accuracy provides information about the probability of a classified pixel actually representing the given class in the reference data, resulting in a value of commission error (CONGALTON 1991; STORY and CONGALTON 1986).

Classified Data	Reference Data F	W	U	Row Total
F	28	14	15	57
W	1	15	5	21
U	1	1	20	22
Column Total	30	30	40	100

Sum of the major diagonal = 63

Overall Accuracy = 63/100 = 63%

Producer's Accuracy
F = 28/30 = 93%
W = 15/30 = 50%
U = 20/40 = 50%

User's Accuracy
F = 28/57 = 49%
W = 15/21 = 71%
U = 20/22 = 91%

Figure 18: Example of a confusion matrix including Producers and Users Accuracy (STORY and CONGALTON 1986: 2).

3. State of the Art

As outlined in chapter 1, research of grassland in combination and/or applied with remote sensing techniques is a well-established field with more than 30 years of experience given by researchers and experts. Hence numerous publications with specific in-depth specializations about this topic exist. This chapter gives a short overview of current research regarding relevant components for this thesis.

Approaches for land cover classification, especially in terms of using random forest classifier can be found e.g. at PAL (2003). His research shows advantages and disadvantages using random forest as a classifier for land cover classification. In his study, PAL presents a comparison of decision tree classifiers and random forest. Results show a nearly equal accuracy of compared classifiers.
GISLASON et al. (2006) explored random forest classifier for land cover classification and its outcomes for multi-source classifications. In their study, they used Landsat multi spectral data, elevation data, slope data and aspect data with the result of outperforming the compared CART-classifier (classification and regression tree) in terms of accuracy and speed.
A comparison of random forest with SVM (support vector machine), neural networks, minimum distance, maximum likelihood and ID3 (decision) tree classifier is provided by KULKARNI and LOWE (2016). Results show an outperforming of all other classifiers given a large number of homogeneous training samples. However, problems and error increase occur with steep slopes in combination with image acquisition time resulting in shadows. In these areas SVM and neural network classifiers could achieve better results than random forest.

With the launch of ESA´s Sentinel satellites, exploitation of free available satellite data increased extraordinarily.
NICULESCU (2018a) presents various approaches using Sentinel-1 data for wetland mapping in the Danube delta. Subsequently, a combination of Sentinel-1 and Sentinel-2 data is used for classification through random forest classifier. His results show a successful approach of change detection regarding wetland restoration.
Suitability of combined Sentinel-1, Sentinel-2 and SPOT-6 satellite data for vegetation monitoring is demonstrated by NICULESCU et al. (2018b). Different approaches including Sentinel-1 time series stacking, SAR images combined with Sentinel-2-derived vegetation indices and combinations of SPOT-6 and SAR data have been carried out. In this study, classification with time series stacking of Sentinel-1, Sentinel-2 and SPOT-6 achieved best results with overall accuracies >90%.
With focus on land use in winter respectively winter vegetation in France, DENIZE et al. (2018) present research undertaken with Sentinel-1 and Sentinel-2 data individual and combined. Combinations of time series were classified with random forest and support vector machine classifiers, resulting in an advantage of Sentinel-2 data over Sentinel-1 data, whereas the combination of SAR- and optical data outperformed both individual products. Furthermore, for improvement of results, DENIZE et al. (2018) suggest the use of very high resolution data due to limitations regarding spatial resolution of Sentinel sensors.

An object-orientated approach for land cover classification in Colombia is demonstrated by CLERICI et al. (2017). Three classifiers, namely SVM, random forest and k-Nearest Neighbor, were tested using Sentinel-1 and Sentinel-2 data. Results show best accuracies for SVM with >85% overall accuracy. Random forest and kNN underperformed with =< 55% accuracy. In terms of image data, CLERICI et al. (2017) especially point out the advantages of combining Sentinel satellite data due all-weather capability from Sentinel-1 SAR sensor and the presence of red-edge bands from optical Sentinel-2 sensor.

CANDIAGO et al. (2015) show an approach of precision farming (PA – precision agriculture) on local scale using UAV-derived vegetation indices. With focus on crop-related issues, the importance and possibilities of vegetation indices, like NDVI, GNDVI and SAVI (see chapter 6.3 Vegetation Indices), not alone regarding agricultural framework is presented.
Research of FRAMPTON et al. (2013) evaluates several Sentinel-2 derived vegetation indices for estimation of biophysical variables like canopy chlorophyll content and leaf chlorophyll concentration. Especially the strength of red-edge bands of S-2 over alternative satellite sensors is pointed out. Further research is particularly suggested in terms green band performance and its impact on chlorophyll estimation.
A study concerning long term vegetation change of southern Iraq is presented by AL-OBAIDEY and AL-BALDAWI (2019). Applied methodologies include an unsupervised classification using NDVI data from 1986 to 2016 resulting in high performance regarding vegetation classification and confirm the use of vegetation indices as an effective appliance to detect various types of vegetation.

Specialized classifications towards grassland can be found e.g. at DOGAN and BOZKURT (2017). Their study examined potential, size and quality of pasture of Isparta province (Turkey) using ASTER data. A combination of laboratory analysis of samples and a remote sensing approach lead to recommendations regarding annual grazing season for farmers and their cattle.
Research of STENZEL et al. (2017) show an examination of high nature value (HNV) grassland. Introduced by the European Union, high nature value grassland is declared as eligible for grants, wherefore monitoring of this protection worthy areas is crucial. Methods include Maxent classifier as well as two types of SVM implicating a separation in several high nature value grassland classes. Best results were accomplished with biased SVM, whereas the differentiation among HNV could not be achieved with approaches tested.
A statistical premised approach using simulated Sentinel-2 data with linear regression vegetation indices and multiple regression reflectance analysis can be found at SAKOWSKA et al. (2016). The objective was an estimation of biophysical parameters, namely seasonal grassland canopy chlorophyll content and photosynthetically absorption from canopy and its photosynthesing components only. Results show promising approaches of grasslands biophysical parameter estimation using various vegetation indices with recommended research towards other ecosystems than grassland.
Research of NUMATA et al. (2007b) include analysis of grassland change detection, more specific pasture degradation/revitalization in Amazonas area Rondônia, Brazil. Methodologies include MODIS and Landsat time series as well as NDVI calculations. Apart from suitability of remote sensing techniques including vegetation indices towards grassland change detection, results also

reveal an insight on environmental circumstances and specific management styles of the counties located in Rondônia.
ESTEL et al. (2018) provide a study of grassland management regimes in Western Europe using MODIS data and NDVI time series. In combination with livestock distribution, information about distinctive cluster of management regimes is obtained. High intensity clusters can be found in Ireland, France and Spain, whereas low intensity cluster are primarily located in Wales and mountainous regions. Within their research, the advantages of remote sensing data and vegetation indices time series in combination with agricultural statistic and the suitability of these methods for grassland monitoring is emphasized.

Regarding grassland classification, numerous studies with various approaches have been carried out using RADAR respectively SAR data.
Research of crop classification including grassland derived by Sentinel-1 SAR time series is published by XU et al. (2018). In multiple Chinese study areas, they show an approach using K-means-clustering towards SAR backscattering responses and various temporal intensity models resulting in high accuracy products in both VH and VV bands regarding crop classification.
HONG et al. (2014) show an approach using combined MODIS and RADARSAT-2 data to differentiate biofuel crop alfalfa from grassland in Canada. With emphasizes towards advantages of their image fusion technique resulting in improvement of accuracy compared to single sensor classification, a challenging aspect of this approach is given due the spatial resolution divergence of 250m (MODIS) and 50m (RADARSAT-2).
VOORMANSIK et al. (2013) show an approach towards detection of grassland cutting practices using polarimetric SAR. In Estonian coastal area, they analyzed various TerraSAR-X backscatter, coherence, entropy and alpha parameters to link grassland management methods with RADAR derived data. Results show no indications of differentiation between short and long grass with threshold 30cm. Although, grass left on the ground after cutting could be detected, further research with various orbits (ascending/descending) and L- or C-band SAR is recommended.
A comparison of TerraSAR-X dual polarimetric and RADARSAT-2 fully polarimetric SAR in terms of grassland cutting practice is presented by VOORMANSIK et al. (2016). Together with a field survey measuring grass height, biomass (wet and dry) and soil moisture, results show high potential of HH/VV polarimetric coherence for the detection of grassland cutting. For future studies, they recommend research using data from promising X- and L-band SAR sensors TanDEM-X and ALOS-2.
Research towards detection of grassland mowing events using Sentinel-1 InSAR data is published by TAMM et al. (2016). Suitability of C-band SAR is shown by an increase of VH and VV polarimetric coherence values right after mowing events. The study also shows the decrease of measured coherence due precipitation and recommendations regarding image acquisition time. For this study Sentinel-1A data with 12-day acquisition was used, leading to author´s recommendation of research using combined Sentinel-1A and 1B data resulting in denser 6-day image pairs.

4. Study Objectives and Research Questions

With the given theoretical background, the motivation and aim of this thesis is

- to investigate the suitability of optical and SAR-data for grassland mapping with an integrated differentiation of intensively and extensively used grassland using Sentinel-1 and Sentinel-2 satellite data.

In consideration to target the above-mentioned objective, the following subordinate research questions will be answered:

i. does the combined use of optical and RADAR data add value in the classification of grassland compared to a single sensor classification?

ii. which from optical sensors derived vegetation indices can be used to estimate mowing events?

iii. to what extent are Sentinel-1 SAR coherences suitable for detecting mowing events?

iv. which advantages/disadvantages using SAR coherences regarding grassland usage intensity classifications compared to VI derived classifications can be detected?

5. Data

This chapter provides an overview of the data used in the thesis. Aside from used satellite data, also reference data, defined area of investigation with its characteristics and sites chosen for detailed analysis are outlined.

5.1. Sentinel Satellite Data

Optical and radar remote sensing data in this thesis are derived by Sentinel-1A/B and Sentinel-2A/B satellite sensors. Sentinel-1 GRD and Sentinel-2 data was already provided and downloaded via Copernicus API Hub. Sentinel-1 SLC data was accessed and downloaded via Copernicus Open Access Hub (https://scihub.copernicus.eu/) using the API-Hub via anaconda environment and python package sentinelsat respectively Alaska Satellite Facility (https://vertex.daac.asf.alaska.edu/) for corrupted data. Table 4 shows an overview of used S-1 and S-2 data.

Table 4: Sentinel-1A/B and Sentinel-2A/B; used data.

Sensor	Usage	Type	Polarization	Orbit	Time span
S-1	Classification	GRD	VV/VH	015; 168	20180101 to 20181231
S-1	Coherence	SLC	VV/VH	015	20180301 to 20180701
S-2	Class./Indices	L2A	-	065	2018

5.2. Reference Data

LUCAS

Developed by the European Commission, the 'Land Use and Coverage Frame Survey' is a standardized and harmonized survey and proceeding to detect land use over EU territory. The survey collects in-situ data, in-field observations are carried out by professional surveyors collecting ground truth data. Due to characteristics of a two-phase sample survey, LUCAS consists of a systematic gathering of points collected with spacing of 2km in northern, eastern, southern and western direction resulting in approximately 1.1 million points covering EU territory. First phase samples include a photo-interpreted assignment to a standardized land cover class whereas second phase samples consist of a field sample including comprehensive soil samples and environmental information (BALLIN et al. 2018: 9ff.; 11f.; 40f.;; EUROPEAN UNION 2017).

IACS/InVeKos

The 'Integrated Administration and Control System', (IACS), in german language also referred as InVeKoS (Integriertes Verwaltungs- und Kontrollsystem) is a policy regarding financing, managing and monitoring of agricultural belongings enacted by the EU and has to be implemented from all participating EU-countries. The IACS regulates income support for farmers based on taxpayer's money in close cooperation with European Agricultural Guarantee Fund (EAGF) and ensures a correctly driven process of transactions regarding agricultural and stockbreeding aid schemes towards the farmers. IACS consists of multiple connected databases – in this thesis, mainly LPIS data

(land parcel identification system) is used to identify agricultural plots within the research area (EUROPEAN PARLIAMENT 2013: 14ff.; EUROPEAN UNION 1995).

5.3. AOI

Tests for classifications and calculations take place in an area of interest with an extent of 40x40km located in tile TNT of the Sentinel-2 tiling grid.

The AOI is located in the western part of Austria, Vorarlberg, and contains urban areas of Bregenz, Dornbirn and outlying parts of Feldkirch. Visual interpretation of satellite imagery shows densely populated areas with the capital city Bregenz (approx. population 30.000) arranged axis-wise in direction northwest and west of the AOI. In the northeast of the AOI, the shoreline of Lake Constance (Bodensee) is visible. About 75% of the area are located in the alpine area of the Central Alps. Due to the alpine character, the topography can be characterized as very pronounced, especially outside of settlement areas. The predominant land cover in the highlands can mostly be described as natural with various forest and meadow species. Settlements are located mainly in the northwest and the valleys of the AOI.

Due to the distinctive topography, also the climatic characteristic of the chosen region is manifold and various regimes with flowing boundaries can be detected. AOIs biggest urban area of Bregenz shows precipitation throughout the whole year with its peak in summer months of June to August. Average temperature is 9.1°C with its peak in July and August with 18°C in average. Coldest month is January with an average temperature of -1°C. The average annual precipitation is 1165mm, whereas February is the driest month with an average of 62mm. As mentioned, precipitation´s peak is during summer months with approximately 135mm/month (Figure 23 and Figure 24).

According to KÖPPEN 1936 and RUBEL et al. 2017 the AOI can be assigned to climate classes Cfb, Dfc and ET (Figure 22). Cfb indicates a warm temperature climate, no dry season (fully humid) and warm summers. Average temperature of all months is below 22°C and there are at least four months with average temperature over 22°C. Parameters for class Dfc are a boreal climate, no dry season (fully humid) and combination of cool summer/cold winter. Class ET indicates polar/alpine climate with no differentiation of seasons like summer and winter (KÖPPEN 1936; KOTTEK et al. 2006; NWS n.d.; RUBEL et al. 2017: 117).

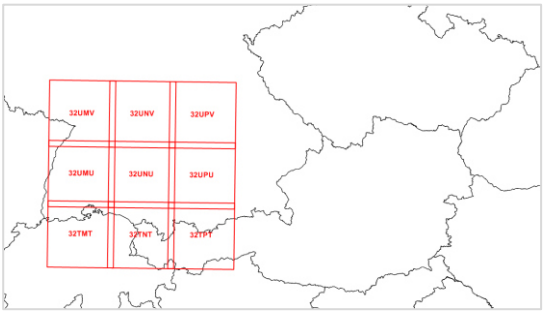

Figure 19: Location of EcoLaSS demo site and AOI.

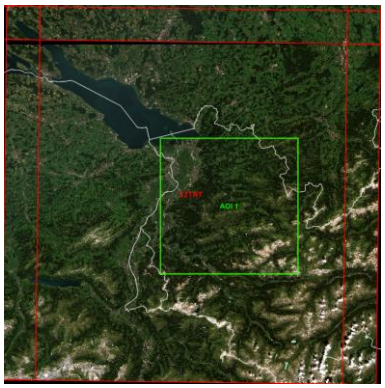

Figure 20: Location of AOIs II.

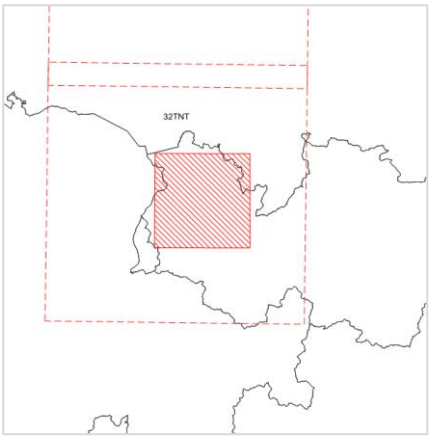

Figure 21: S-2 tile TNT with location of AOI..

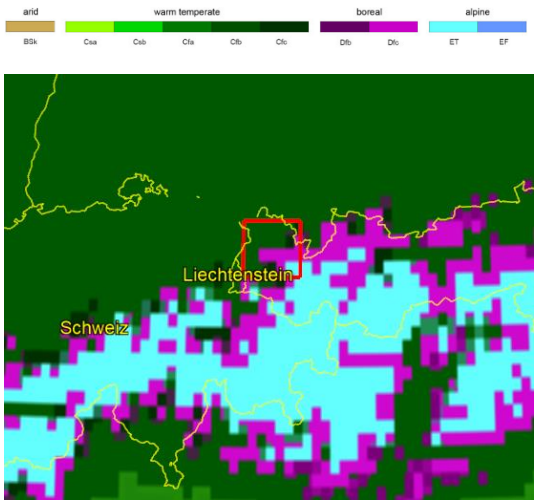

Figure 22: Climate Classes of AOI (Rubel et al. 2017).

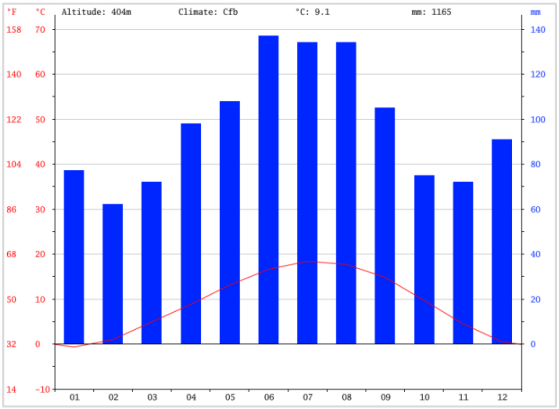

Figure 23: Climate Graph of Bregenz (https://en.climate-data.org/).

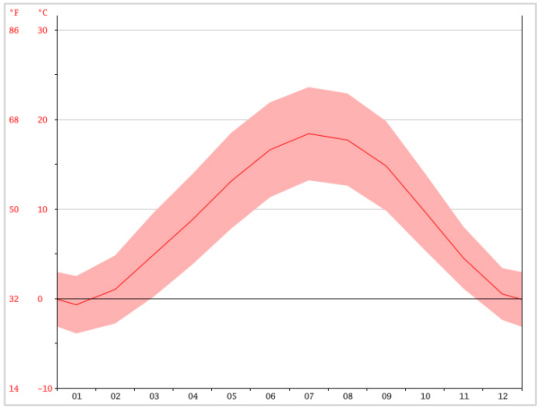

Figure 24: Yearly Average Temperature of Bregenz (https://en.climate-data.org/).

5.4. Sites

Four sites within AOI have been selected for extraction of time series from vegetation indices and coherence estimation (Figure 25 to Figure 28; scale 1:10.000). The sites were defined as polygons from IACS respectively InVeKos data and declared with a buffer of -10m to increase homogeneity due to exclusion of areas consisting of mixed pixels at polygons borders. Sites were chosen in consideration to equally cover the spectrum of intensive and extensive used grassland using reference data – resulting site 1 and 3 as intensive and site 2 and 4 as extensive used grassland. Table 5 presents key figures of each site. Site areas show a range from 6.178sqm to 21.057sqm and are located between 490m and 980m altitude above sea level. With the chosen sites, a relation between area and altitude, e.g. the higher the altitude, the smaller the site, cannot be detected.

Figure 25: Site 1.

Figure 26: Site 2.

Figure 27: Site 3.

Figure 28: Site 4.

Table 5: Key figures of sites.

	Coordinates	area sqm	altitude m
Site 1	47°13’56.84”N, 9°52’54.52”E	21.057	850
Site 2	47°25’40.95”N, 9°59’24.58”E	6.178	950
Site 3	47°11’56.58”N, 9°40’18.07”E	14.384	490
Site 4	47°25’17.20”N,10° 0’40.10”E	13.104	980

6. Methodology

In this chapter, the applied methods for answering the research questions are outlined. This includes the definition of grassland use intensity as well as the processing workflow from the input data towards the classification process up to the availed validation.

6.1. Grassland Usage

As a principle for the classification or differentiation between extensively and intensively used grassland, D33.1a – Time Series Analysis for Thematic Classification (GAF AG 2018) respectively HRL grassland 2015, is used and described by the following characteristics:

ELEMENTS TO BE INCLUDED IN THE GRASSLAND PRODUCT	ELEMENTS TO BE EXCLUDED FROM THE GRASSLAND PRODUCT
▪ Natural, semi-natural, agricultural / managed grass-covered surfaces ▪ Grasslands with scattered trees and shrubs covering a maximum 10% ▪ Heathland with high grass cover, maximum of 10% non-grass cover ▪ Coastal grasslands, such as grey dunes and salt meadows located in intertidal flat areas with at least 30% graminoid species of vegetation cover ▪ Sparsely vegetated grasslands (>30% vegetation cover – cf. comment below) ▪ Grasslands in urban areas: parks, urban green spaces in residential and industrial areas ▪ Semi-arid steppes with scattered Artemisia scrub ▪ Meadows: grassland which is not regularly grazed by domestic livestock, but rather allowed to grow unchecked in order to produce hay ▪ Grasslands in urban areas: sport fields, golf courses ▪ Grasslands on land without use ▪ Natural grasslands on military sites	▪ Peat forming ecosystems dominated by sedges ▪ Reed beds and helophytes dominated systems ▪ Tall forbs, fern, shrub dominated vegetation ▪ Grasslands that have been observed as tilled (in the reference year or a certain period before, in that case they are considered as arable fields) ▪ Rice fields ▪ Vineyards, orchards, olive groves, (if more than 10% shrubs or trees) ▪ Tundra dominated by shrubs and lichens ▪ Grassland on fresh (and older) clear-cuts in the woods

Figure 29: Definition of Grassland according to the HRL 2015 (GAF AG 2018, 17)

Based on Figure 29, a further subdivision into extensively and intensively used grassland takes place. In multitemporal analysis, the intensity of grassland usage is mainly determined by the following indicators: i) mowing frequency, ii) pasture intensity and iii) amount of fertilizer used (GÓMEZ GIMÉNEZ et al. 2017). Biodiversity-friendly, low intensity pasture farming generally requires little anthropogenic intervention, e.g. permanent grassland is manageable with one mowing event p.a. to prevent the growth of shrubs and trees. Intensively used grasslands on the other hand, are characterized by a higher mowing frequency, a higher stocking density and, in general, a much higher use of added nutrients and agrochemicals (KOLECKA et al. 2018).

In consideration of the mentioned indicators, and the necessity of measurability with remote sensing methods in combination with time series analysis, the main criteria for distinction of intensively and extensively usage of grassland is the number of mowing events respectively the mowing frequency and the time of execution of the mowing event.
In recommendation of BEKKEMA and ELEVELD 2018: 195; EUROPEAN COMMISSION 2013: 80; FRANKE et al. 2012: 126f.; GÓMEZ GIMÉNEZ et al. 2017: 127f.; KEUCK et al. 2010; KOLECKA et al. 2018: 3; SCHIRPKE et al. 2017, intensive use of grassland is defined by:

- First cuts/mowing events end of April/begin of May
- Minimum of three cuts per season
- occur at 1500m a.s.l. max

whereas characteristics of extensively used grassland are

- no cuts until July
- less than three cuts per growing season
- located above and beneath 1500 a.s.l.

6.2. Satellite Data Preprocessing

Satellite data preprocessing was undertaken by GAF AG due existing project environment and program specifications and has been applied to data used.
Access point of Sentinel-2 data from 01/01/2018 to 01/11/2018 is CopernicusHub via sentinelsat-tool. Radiometric correction, topographic normalization, calibration, cloud mask and quality metrics is applied with sen2cor and internal software.
Sentinel-1 GRD data from 01/01/2018 to 01/11/2018 is also derived via CopernicusHub using sentinelsat-tool. Images of orbit 15 (ascending) and 168 (descending) have been undertaken radiometric calibration, terrain flattening, coregistration/stacking and multitemporal speckle filtering using SNAP.

6.3. Vegetation Indices

With Sentinel-2 data, spectral (vegetation)indices in terms of information gain have been calculated. The calculation took place per pixel and several bands of the multispectral S-2-sensor were used to generate 6 indices.

NDVI
The Normalized Difference Vegetation Index is one of the most popular indices to detect vegetation, analyze its development, photosynthetic activity and vitality. Provided by ROUSE and HAAS (1974), the NDVI makes use of reflectance in the near infrared and red band, and is calculated with the equation:

$$NDVI = \frac{NIR - RED}{NIR + RED}$$

The result of the calculated NDVI provides values between -1 and +1, whereas a value near +1 indicates dense and healthy vegetation, values near 0 imply bare soil and negative values water, snow or clouds. Using the NDVI, the common values for vegetation range between .2 and .9 (CANDIAGO et al. 2015; FARAMARZI et al. 2018). In the given case of using Sentinel 2 data, band 04 and 08 were used for the calculation.

GNDVI

The Green Normalized Difference Vegetation Index is a modified version of the NDVI. Instead of the red band, like the NDVI, it uses the green band resulting in a higher sensitivity regarding the chlorophyll content of the vegetation (CANDIAGO et al. 2015; GITELSON et al. 1996). The GNDVI is calculated with following equation:

$$GNDVI = \frac{NIR - GREEN}{NIR + GREEN}$$

Using Sentinel 2 data, NIR and GREEN are declared with band 03 and band 07.

IRECI

The inverted red edge chlorophyll index (IRECI) was introduced by FRAMPTON et al. (2013) in a study about the estimation of canopy chlorophyll content and leaf chlorophyll concentration. IRECI takes advantage of the red edge bands (B5 and B6) of the S-2 MSI, while also including near infrared and red band in its calculation. Its equation is as follows using S-2MSI band 04, 05, 06 and 07:

$$IRECI = \frac{(NIR - RED)}{(RE1/RE2)}$$

EVI

With the launch of MODIS (moderate resolution image sensor) on satellites TERRA and AQUA, also the enhanced vegetation index (EVI) has been published. Especially for MODIS-data, the EVI aims to correct canopy background and atmospheric influences towards MODIS NDVI calculations (AREKHI et al. 2019: 5f.; HUETE et al. 1999: 11f.; NASA n.d.).

$$EVI = 2.5\ x\ \frac{(NIR - RED)}{(NIR + 6RED - 7.5BLUE + 1)}$$

EVI2

Provided by JIANG et al. (2008), enhanced vegetation index 2 (EVI2), also called 2-band EVI, is developed especially for sensors without a blue band. Using only red and near infrared bands it is defined as:

$$EVI2 = 2.5\ x\ \frac{(NIR - RED)}{(NIR + 2.4RED\ + 1)}$$

SAVI

Introduced by HUETE (1988) , SAVI (soil-adjusted vegetation index) takes consideration of soil brightness influences of indices using red and near infrared bands. With inclusion of these soil derived parameters quality could be enhanced especially regarding global models of soil-vegetation systems (HUETE 1988).

$$SAVI = 1.5x\frac{NIR - RED}{NIR + RED + 0.5}$$

6.4. Training and Test Data

Samples for training and test data in order to compute the land cover classification, respectively the general grasslandmask, were provided in-house by GAF AG. The classification contains 6 classes and is also used in previous products of the program. The 6 classes are: broadleaf trees (1), coniferous trees (2), urban/impervious (3), water (4), grassland (5) and cropland (6). 200 samples of 30x30m, respectively 3x3 pixels, for each of the 6 classes were generated along a 2km spacing grid and assigned to the corresponding class extracted from previous EcoLaSS-product HRL 2015 (High Resolution Layer 2015). Samples were allocated to homogeneous areas, so no sample is taken in mixed-pixel-sections.

6.5. Time Feature Calculation

In terms of a meaningful classification of the general grassland class, the foregoing classification was executed with multiple time features including the minimum value, maximum value, standard deviation (SD), percentiles 10, 25, 50, 75, 90, difference of percentiles 75-25 and 90-10, of NDVI, NDWI, IRECI and Brightness for multiple time spans. Time periods include all available Sentinel-2 images for the year 2018 and Sentinel-2 images for the first half of the year 2018, respectively 01 January to 01 June as well as 01 March to 01 June. Three timespans have been chosen to obtain a better separation of classes grassland and cropland due to a different growing season resulting in a variance of their spectral signature.

In addition to the mentioned time feature extraction of optical Sentinel-2 data, also Sentinel-1 time features including minimum value, maximum value, standard deviation, percentiles 10, 25, 50, 75, 90, difference of percentiles 75-25 and 90-10 for polarizations VV, VH and Normalized Difference of VVVH (NDVVVH) as well as the Ratio of VVVH for three time spans of year 2018 were calculated. Table 6 shows a detailed listing of calculated time features and time spans for each band.

Table 6: Calculated Time Features.

S2		
BANDS	**FEATURES for each band**	**DATE for each band**
NDVI	Min	20180101 – 20181231
NDWI	Max	20180101 – 20180601
IRECI	SD	20180301 – 20180601
BRIGHTNESS	Percentiles 10, 25, 50, 75,90, diff 75 25, diff 90 10	
S1		
BANDS	**FEATURES for each band**	**DATE for each band**
VV	Min amplitude	20180101 – 20181231
VH	Max amplitude	20180101 – 20180601
VH-VV	SD	20180301 – 20180601
NDVVVH	Percentiles 10, 25, 50, 75,90, diff 75 25, diff 90 10	

6.6. Landcover Classification

The classification was executed with a random forest classifier (discussed in 2.3.1) using eolearn, a collection of python packages for specific tasks regarding satellite imagery. Input data were variations of calculated time features shown in Table 6 and the sample file discussed in chapter 5.2 and 6.4.

From the resulting classification, class grassland respectively a grassland mask has been extracted. Further classification for grassland use intensity took place based on this grassland mask.

6.7. Classification – Grassland Use Intensity

6.7.1. Sentinel-1 SLC coherence calculation

The estimation of the grassland use intensity was executed with a before going calculation of SAR-coherence. For each coherence image product, a pair of SLC images, one assigned as master and the other as slave, were used as input. The detailed workflow is shown in Figure 30.

First step was the process of coregistering the input images, which is summarized as individual steps “TOPSAR-Split”, “Apply Orbit File” and “Back-Geocoding”. With TOPSAR-Split a separation of the three sub-swaths is achieved. “Apply Orbit File” sets the Orbit Auxiliary Data for the given image. This information contains precise data about the satellite position during the acquisition. In the process of “Back-Geocoding” the used digital elevation model (DEM) and interpolation methods are defined. In this workflow SRTM-DEM (Shuttle Radar Topography Mission) with a spatial resolution of 30m was used.

Processing step “Interferogram” computes the actual calculation of interferometric coherence between designated master and slave images by cross multiplying the amplitudes of the images (see chapter 2). “TOPSAR-Deburst” and “TOPSAR-Merge” are causing a join, respectively a merge of each burst (deburst) and sub-swaths. To reduce speckle appearance, process of “multilook-filtering” is applied to the interim result. Last step of the process applies “terrain correction” using mentioned SRTM-DEM with 30m resolution to correct geometry effects as discussed in chapter 2.

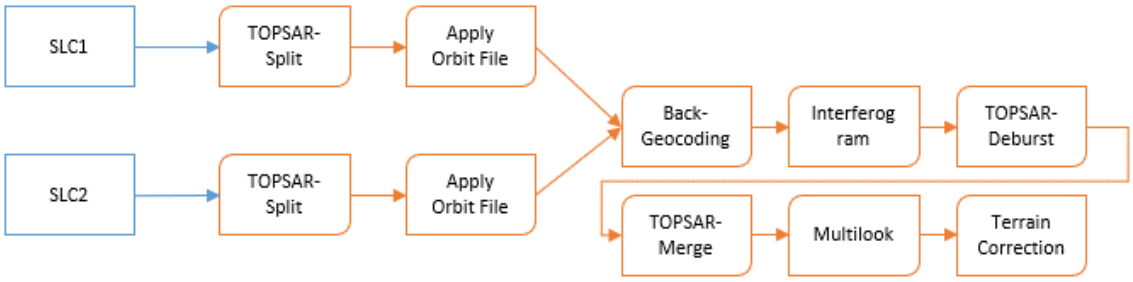

Figure 30: Workflow for interferometric coherence calculation.

For the classification via SVM-classifier, 100 samples per intensive/extensive class were collected. Samples were set, likewise to general landcover classification (chapter 6.4), as 3x3 pixel polygon in the center of reference polygons (IACS).

6.7.2. Sentinel-2 NDVI calculation

In addition of the coherence calculation, an estimation of mowing events was computed using NDVI. After analyzing the data, thresholds were set to exclude clouds and snow due to falsification and non-applicability.

Two approaches were applied using optical data. First approach used minimum (mean) values per month of calculated NDVI, while the second approach made use of a calculation of differences per NDVI-scene. Each approach results in a detection of mowing event in the given timespan (month or scene). To obtain a differentiation in extensive and intensive usage, all calculations were reclassified to value 0 (no mowing event) respectively value 1 (mowing event) and summarized, separated in time spans from March to July and July to November, to verify the result corresponding to given grassland definition in chapter 6.1. An illustration of this process is shown in Figure 31.

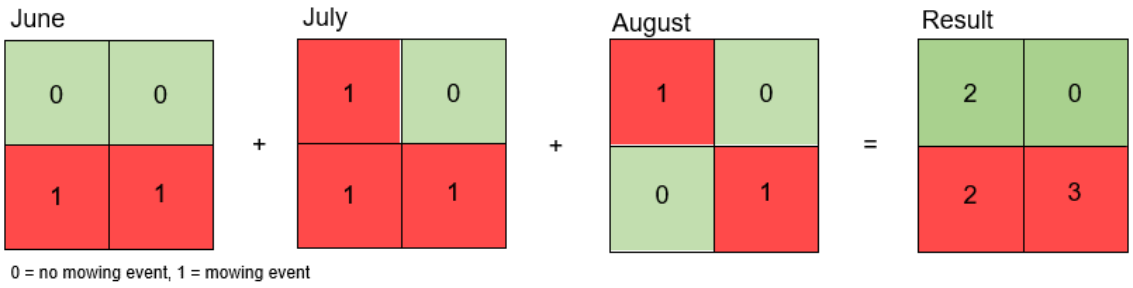

Figure 31: Scheme of ext/int classification process.

NDVImin (mean) per month

For the first approach to estimate mowing events, the mean of NDVImin per month from March to September was calculated. Standard deviations (SD) for each month have been computed to assume a mowing occurrence. In this research, thresholds of .25 and 1 standard deviation have been used, leading to an assumption of a mowing events for each pixel with a deviance of ≤ .25 SD and ≤ 1 SD of the mean NDVImin from the previous month. Pixels with given deviance were reclassified to value 1 (all other 0).

NDVI difference per scene

For the second approach, the difference of each NDVI-scene was calculated. After visual inspection of the calculated images, a threshold for differences >3 SD was defined for the occurrence of clouds, resulting in an exclusion of the given pixels. For each scene, another threshold was set at 1 standard deviation. Changes ≤1 SD to the previous scene were assumed to be a mowing event. Furthermore, a reclassification took place where these values were assigned to value 1 (all other 0).

6.7.3. Post-classification processing

The classification results were undertaken operational steps of an exclusion (reclassification) based on elevation, filtering and an elimination of small regions due to homogeneity.

Due definition of extensive/intensive used grasslands (Chapter 6.1) and the given predominant topographical characteristics of the location of interest (LOI), the threshold for a possible intensive grassland management is declared to a restricted elevation of 1500m asl.

To reduce small clusters of pixels respectively speckles and for a homogeneous result, a filter of 5x5px was applied to the result of the classification. Furthermore, a mask with areas smaller than 25px was created and intersected with the 5x5 filtered image. This step allowed an extraction of any extant single or small groups of mainly edge-pixels, leading to a homogeneous result of the bicategorical classification.

Figure 32 illustrates the complete workflow in addition to methodologies for the different approaches regarding grassland use intensity classification previously discussed.

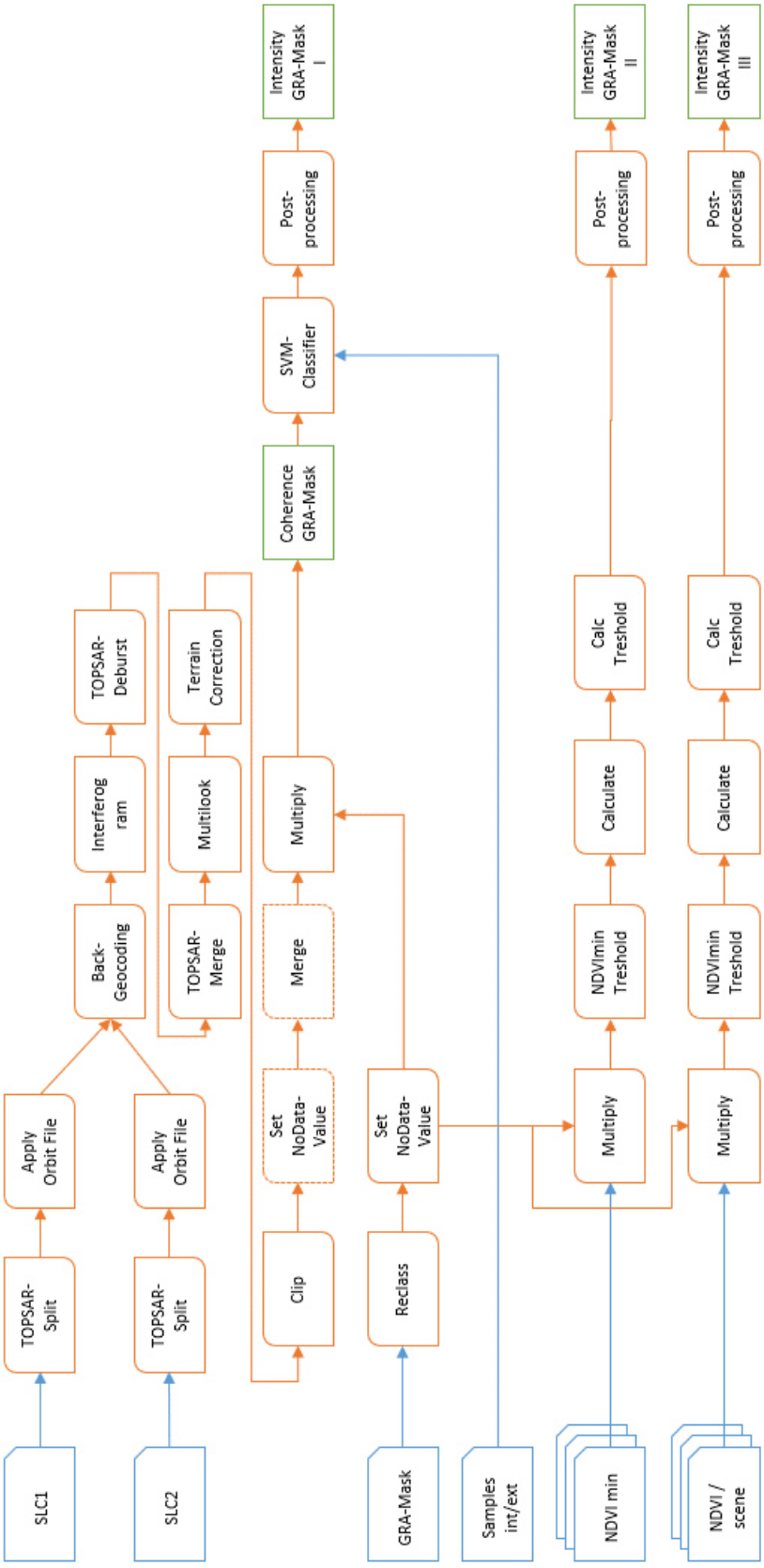

Figure 32:Workflow of grassland use intensity classifications.

6.8. Accuracy Assessment and Reference Data Preparation

Accuracy Assessment for use intensity classification was carried out using IACS-polygons. For each IACS site, the mean center for attribute extraction was created.

Regarding the appointed definition in chapter 6.1, features with attribute “hay meadow/ -pasture with three or more usages” (IACS/INVEKOS term:”Mähwiese/ -weide drei und mehr Nutzungen”) were considered as intensively used grassland, whereas features with attributes “hay meadow/ -pasture with two usages” (“Mähwiese/ -weide zwei und mehr Nutzungen”), “single hay meadow” (“einmähdige Wiese”) and “alpine pasture” (“Almfutterfläche”) were handled as extensive used grassland.

For an attribute join, the raster of the classification result was transformed in a vector layer. With the resulting feature class, respectively its attribute table, a comparison of the classified data and the reference data took place and confusion matrices have been created. In addition to overall accuracy, also Cohen´s Kappa, user´s and producer´s accuracy have been calculated.

Regarding to LANDIS and KOCH (1977), Kappa is a quantitative measurement of reliability respectively it measures the agreement between raters, in this case land cover classes as well as intensively and extensively used grassland. Values reach from 0 to 1 where the higher Kappa the better the agreement. Categoric benchmarks of Kappa are shown in Table 7.

Table 7: Kappa: Benchmarks (LANDIS and KOCH 1977: 165)

Kappa Value	Agreement
0.00	Random
0..01 – 0.20	Slight
0.21 – 0.40	Fair
0.41 – 0.60	Moderate
0.61 – 0.80	Substantial
0.81 – 1.00	Almost Perfect

7. Results

The following chapter presents the results of the various classifications using different sensors, timespans and approaches. Chapter 7.1 represents the output for the primary classification to obtain a general grassland mask including confusion matrices of all single- and multi sensor classifications and the visualization of the best result.
Furthermore, detection of mowing events with calculated vegetation indices and interferometric coherence determination as well as maps of grassland use intensity with their confusion matrices are presented and explained.

7.1. Landcover Classification

Following tables show the confusion matrices of land cover classifications with 6 classes derived by single sensor Sentinel-1 or Sentinel-2 remote sensing data.
Table 8 and Table 9 present the accuracy assessment obtained from Sentinel-1 data over two timespans. S-1 classification with data from 01.01 to 31.12. (Table 8) achieved an overall accuracy of .69 with Kappa value .62. Inaccurate assignation occurs especially at classes 1 and 2, respectively the two classes broad-leafed and conifer tree cover with PA and UA values at around .5. The detection of class water with Sentinel-1 radar sensor is nearly without limitations or mismatches. Grassland classification achieved values of PA and UA of .74 and .69, where the biggest instability refers to class 6 cropland.

Table 8: Accuracy Assessment S-1 01.01.-31.12.

S1 20180101 – 20181231									
		Reference data							
		1	**2**	**3**	**4**	**5**	**6**	**sum**	**UA**
Classification	**1**	**501**	311	144	0	47	26	1029	0.49
	2	230	**484**	83	1	46	14	858	0.56
	3	78	77	**566**	0	30	2	753	0.75
	4	0	0	1	**646**	12	2	661	0.98
	5	73	40	76	0	**745**	148	1082	0.69
	6	44	14	42	0	128	**726**	954	0.76
	sum	926	926	912	647	1008	918	**5337**	-
	PA	0.54	0.52	0.62	1.00	0.74	0.79	-	-
1: broad leafed tree; 2: conifer tree; 3: imperviousness; 4: water; 5: grass; 6: crop								**Overall**	**0.69**
								Kappa	**0.62**

In comparison, S-1 classification with time span 01.01 to 01.06 (Table 9) obtains an enhancement with OA of .8 and Kappa .76. In terms of the individual classes, almost all accuracies underlie an improvement, which refers especially to classes broad-leafed and conifer tree cover. Improvements of grasslands are shown with PA .77 and UA .76. As in Table 8, misinterpretations occur primarily with class crop – which shows a drop at PA to an accuracy of .67 with risen instabilities regarding classes 1, broad-leafed trees and 3, imperviousness.

Table 9: Accuracy Assessment S-1 01.01.-01.06.

S1 20180101 – 20180601									
		Reference data							
		1	**2**	**3**	**4**	**5**	**6**	**sum**	**UA**
Classification	**1**	**663**	79	30	0	48	107	927	0.72
	2	144	**815**	6	0	32	3	1000	0.82
	3	41	6	**743**	0	57	94	941	0.79
	4	0	0	0	**647**	5	0	652	0.99
	5	40	23	73	0	**774**	103	1013	0.76
	6	38	3	60	0	92	**611**	804	0.76
	sum	926	926	912	647	1008	918	**5337**	-
	PA	0.72	0.88	0.81	1.00	0.77	0.67	-	-
1: broad leafed tree; 2: conifer tree; 3: imperviousness; 4: water; 5: grass; 6: crop								**Overall**	**0.80**
								Kappa	**0.76**

Table 10 and Table 11 present single sensor classification using Sentinel-2 data. Using time span 01.01. to 31.12., the S-2 classification achieved an OA of .87 with a Kappa value of .84. As with the S-1 classifications, the least accurate allocations take place in classes broad-leafed tree cover regarding an UA and PA of .8 respectively .75. Classification of grassland reaches PA and UA values of .8 and .83. The most precise assignment is related to class 4, water, with PA and UA 1.

Table 10: Accuracy Assessment S-2 01.01.-31.12.

S2 20180101 – 20181231									
		Reference data							
		1	**2**	**3**	**4**	**5**	**6**	**sum**	**UA**
Classification	**1**	**698**	91	9	0	69	10	877	0.80
	2	124	**826**	2	0	26	3	981	0.84
	3	39	3	**863**	1	48	17	971	0.89
	4	0	0	1	**646**	0	0	647	1.00
	5	60	6	18	0	**802**	81	967	0.83
	6	5	0	19	0	63	**807**	894	0.90
	sum	926	926	912	647	1008	918	**5337**	-
	PA	0.75	0.89	0.95	1.00	0.80	0.88	-	-
1: broad leafed tree; 2: conifer tree; 3: imperviousness; 4: water; 5: grass; 6: crop								**Overall**	**0.87**
								Kappa	**0.84**

Compared to Table 10, Table 11 shows the land cover classification with S-2 data applied with time spans 01.01. to 31.12. and 01.01. to 01.06. overall accuracy of .88 and Kappa of .85 reveal an improvement over one-period classification using Sentinel-2 data, with an enhancement especially in class grassland (PA .84; UA .85).

Table 11: Accuracy Assessment S-2 01.01.-31.12 & 01.01.-01.06.

S2 20180101 – 20181231									
S2 20180101 – 20180601									
		Reference data							
		1	**2**	**3**	**4**	**5**	**6**	**sum**	**UA**
Classification	**1**	**691**	87	12	0	37	15	842	0.82
	2	136	**825**	1	0	38	3	1003	0.82
	3	36	4	**871**	1	35	16	963	0.90
	4	0	0	0	**646**	0	0	646	1.00
	5	58	8	12	0	**849**	72	999	0.85
	6	5	2	16	0	49	**812**	884	0.92
	sum	926	926	912	647	1008	918	**5337**	-
	PA	0.75	0.89	0.96	1.00	0.84	0.88	-	-
1: broad leafed tree; 2: conifer tree; 3: imperviousness; 4: water; 5: grass; 6: crop								**Overall**	**0.88**
								Kappa	**0.85**

In Table 12 the multi sensor classification using Sentinel-1 and Sentinel-2 data is shown. This classification combines the previous three classifications of S-1 01.01-31.12; S-2 01.01-06.01 and S-2 01.01-31.12. and achieved an overall accuracy of .88 with Kappa value .85.
Most accurate class in this classification is, like in the previous ones, class water with UA and PA 1. Regarding the tree cover classes an UA and PA of .82 (broad-leafed and conifer) and .73 (broad leafed) respectively .9 are reached. Classes grassland and crop show values for UA and PA with .85 and .83 for grassland respectively .88 and .89 for cropland.

Table 12: Accuracy Assessment S-1 01.01.-31.12 and S2 01.01.-31.12 & 01.01.-01.06.

S1 20180101 – 20181231									
S2 20180101 – 20180601									
S2 20180101 – 20181231									
		Reference data							
		1	**2**	**3**	**4**	**5**	**6**	**sum**	**UA**
Classification	**1**	**678**	82	12	0	38	12	822	0.82
	2	136	**831**	3	0	39	4	1013	0.82
	3	31	3	**859**	1	40	8	942	0.91
	4	0	0	1	**646**	0	0	647	1.00
	5	64	6	6	0	**836**	73	985	0.85
	6	17	4	31	0	55	**821**	928	0.88
	sum	926	926	912	647	1008	918	**5337**	-
	PA	0.73	0.90	0.94	1.00	0.83	0.89	-	-
1: broad leafed tree; 2: conifer tree; 3: imperviousness; 4: water; 5: grass; 6: crop								**Overall**	**0.88**
								Kappa	**0.85**

Figure 33 to Figure 35 show the result of the classification used as a basis for the continuous differentiation in extensively and intensively used grassland – classification #4 (Table 11) came into

use. Figure 33 presents the classification showing all 6 classes. Pixels in the upper left corner classified as water represent Bodensee and its tributary, river Rhine (Rhein). Imperviousness areas are detectable along the urban areas in the west, along valleys and mountainous, rocky areas in the south-east. Forest and grassland are distributed evenly over the extent, whereas grassland shows focal points in mountainous areas (center and east) and in-between the urban areas near Bodensee. Figure 34 and Figure 35 illustrate the grasslandmask only, once with a Sentinel-2 scene from August 25 as base layer and once the plain mask of AOI without base layer or background image.

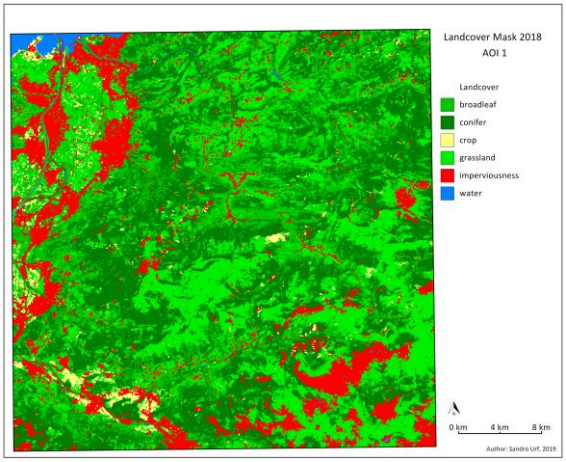

Figure 33: Land Cover Classification (all classes).

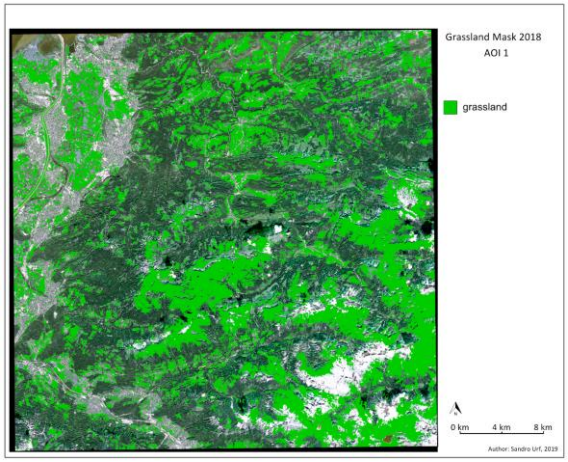

Figure 34: Land Cover Classification (Grasslandmask).

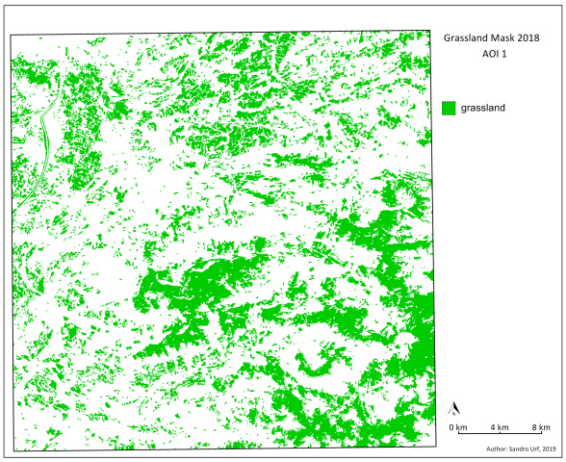

Figure 35: Grasslandmask

7.2. Detection of Mowing Events

7.2.1. Timeseries of Indices

Timeseries of indices (Figure 36 to Figure 39) show the comparison for each site over time span of 2018. Compared to behavior of NDVI, all other indices, GNDVI, EVI, EVI2, IRECI and SAVI, behave in nearly similar manner. This is confirmed in the correlation matrix (Table 13), where all indices and their correlations with NDVI are shown. With minor differences throughout the sites, all indices indicate a strong positive correlation. Correlation values for most cases are >.9; the

lowest value shows a correlation of .85. The red line indicates 1st of July as one criterion for the differentiation of grassland management schemes (chapter 6.1).

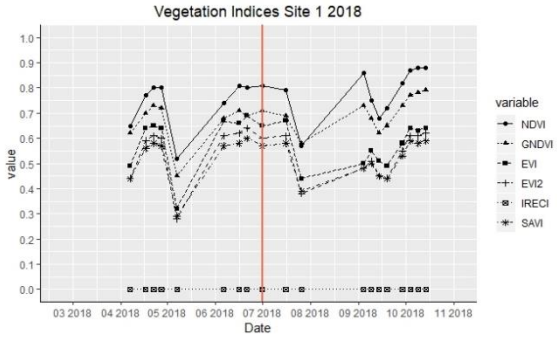

Figure 36: Vegetation Indices Site 1 2018

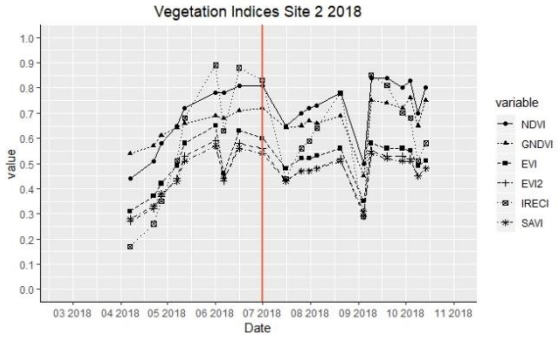

Figure 37: Vegetation Indices Site 2 2018

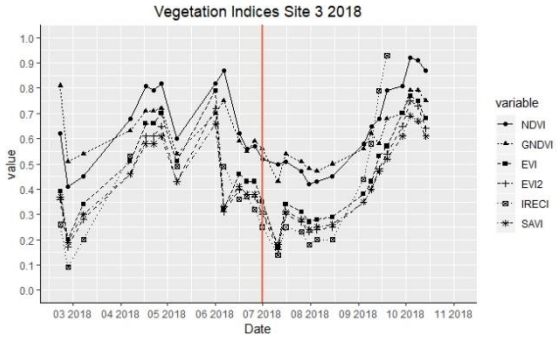

Figure 38: Vegetation Indices Site 3 2018

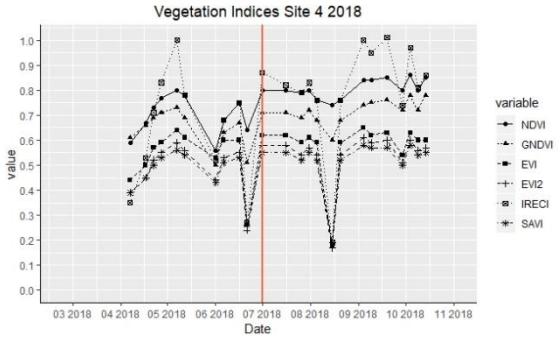

Figure 39: Vegetation Indices Site 4 2018

Table 13: Correlation Matrix of Indices based on NDVI.

Site1	GNDVI	EVI	EVI2	IRECI	SAVI
NDVI	.99	.96	.97	.93	.98
Site2					
NDVI	.99	.97	.99	.95	.99
Site3					
NDVI	.94	.87	.90	.85	.91
Site4					
NDVI	.99	.90	.93	.91	.94

7.2.2. Interferometric Coherence

Examples for detection of mowing events are shown in exemplary sites at Figure 40 to Figure 45. Each pair of images shows one timespan with low coherence, indicating no occurrence of a mowing event, and another timespan with high coherence, betoken as an appearance of a mowing event. A detailed discussion regarding the shown images is undertaken in Chapter 8.3.

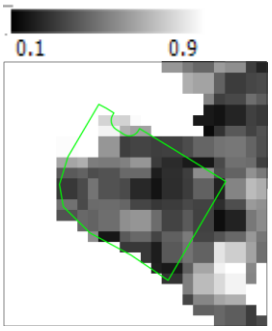

Figure 40: Inferometric Coherence 13/03 to 19/03.

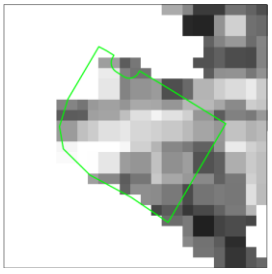

Figure 41: Inferometric Coherence 30/04 to 06/05.

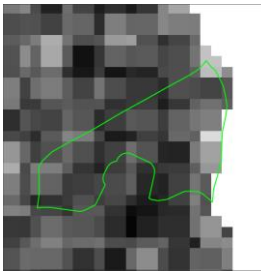

Figure 42: Inferometric Coherence 07/03 to 13/03.

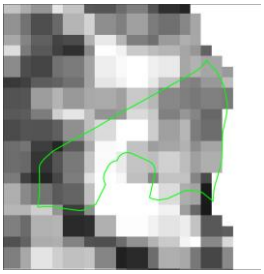

Figure 43: Inferometric Coherence 24/04 to 30/04

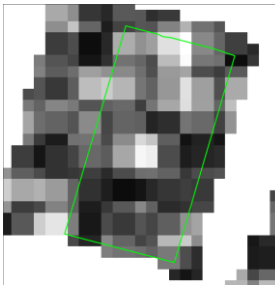

Figure 44: Inferometric Coherence 11/06 to 17/06.

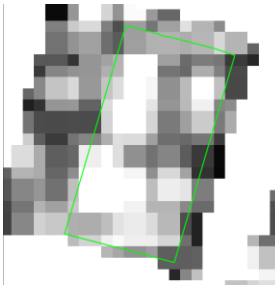

Figure 45: Inferometric Coherence 17/06 to 23/06.

7.3. Classification – Grassland Use Intensity

Following tables and figures show the confusion matrices and visualizations of grassland use intensity maps. Each map also includes detailed extents of the sites, from which also vegetation indices have been calculated (chapter 7.2.1). A detailed discussion of site-classification takes place in chapter 8.3.1.

Interferometric Coherence VV

Use intensity classification with polarization VV reached and overall accuracy of .69 with a Kappa value of .31. Outcomes for user´s accuracy attain values of .43 for extensive use and .86 for intensive use. Values for producer´s accuracy reach .67 for extensive and .69 for intensive use of grassland. Out of 20.536 validations, 14.108 are assigned to the correct class (Table 14). Figure 46 shows the corresponding map of the classification.

Table 14: Accuracy Assessment InSAR Coherence VV

		Reference Data			
Classification		**Ext 0**	**Int 1**	**sum**	**UA**
	Ext 0	**3601**	4680	8281	0.43
	Int 1	1748	**10507**	12255	0.86
	sum	5349	15187	**14108**	-
	PA	0.67	0.69	-	-
				Overall	**0.69**
				Kappa	**0.31**

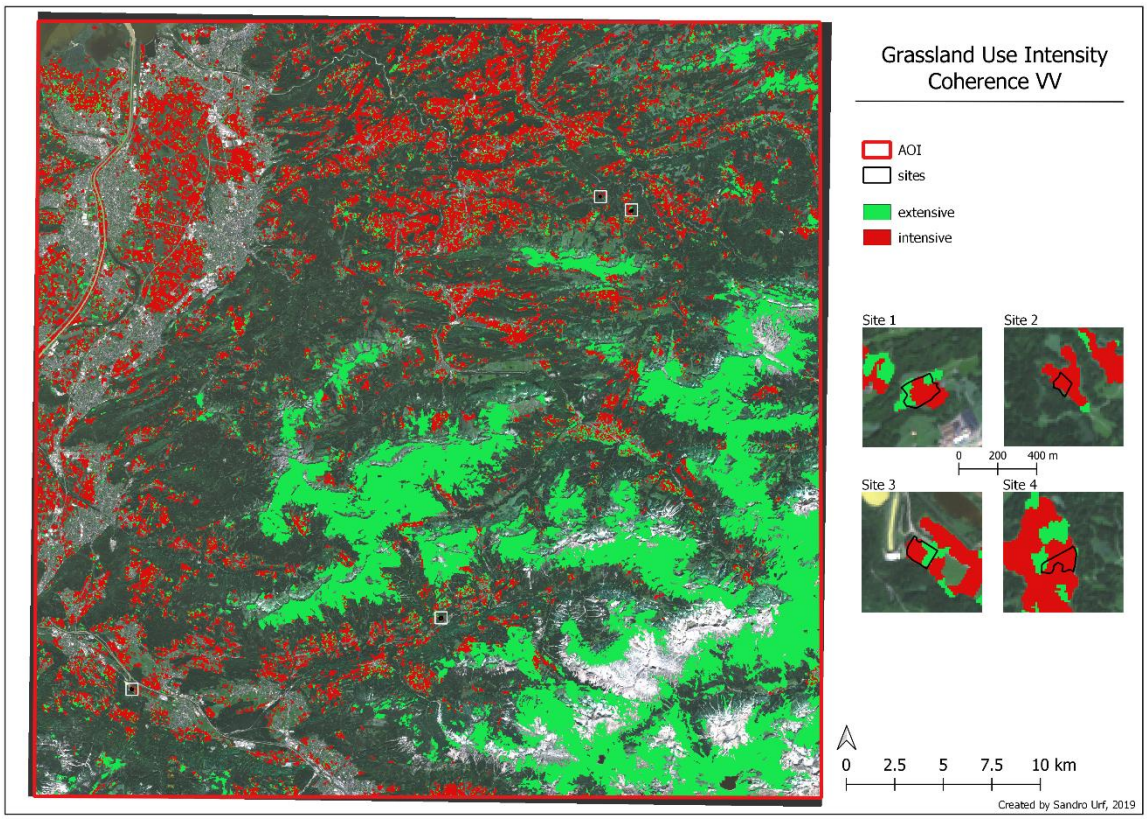

Figure 46: Grassland Use Intensity Coherence VV.

Interferometric Coherence VH

The second classification using SAR-coherence data reached an overall accuracy of .68 with Kappa .30. Compared to the results of VV-polarization, producer´s and user´s accuracy deteriorated modest. UA reaches .42 respectively .86 for extensive and intensive use, while PA´s values remain identical as with SAR-VV data as aforesaid, .67 and .69 (Table 15). The complementary map is shown in Figure 47.

Table 15: Accuracy Assessment InSAR Coherence VH

		Reference Data			
Classification		**Ext 0**	**Int 1**	**sum**	**UA**
	Ext 0	**3390**	4723	8113	0.42
	Int 1	1642	**10427**	12069	0.86
	sum	5032	15150	**13817**	-
	PA	0.67	0.69	-	-
				Overall	**0.68**
				Kappa	**0.30**

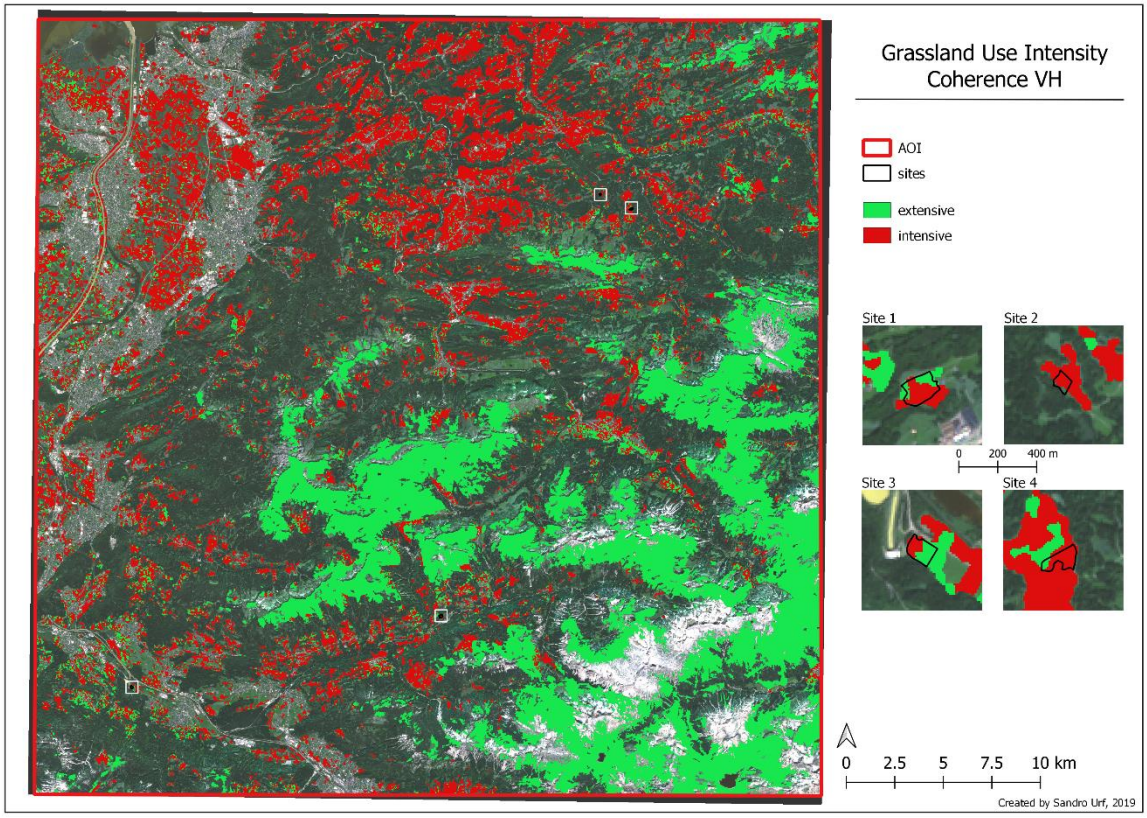

Figure 47: Grassland Use Intensity Coherence VH.

NDVI diff

The first use intensity classification based on NDVI calculation, respectively the difference per scene reached an overall accuracy of .65 with Kappa .30. User´s accuracy achieved .7 for extensive class and .61 for intensive class, while producer´s accuracy reached .55 and .75 for extensive and intensive usage. Altogether 13.338 validations were assigned to the correct class (Table 16). Figure 48 shows the corresponding map of the classification.

Table 16: Accuracy Assessment NDVI diff/scene

		Reference Data			
		Ext 0	**Int 1**	**sum**	**UA**
Classification	**Ext 0**	**5801**	2480	8281	0.70
	Int 1	4728	**7537**	12265	0.61
	sum	10529	10017	**13338**	-
	PA	0.55	0.75	-	-
				Overall	**0.65**
				Kappa	**0.30**

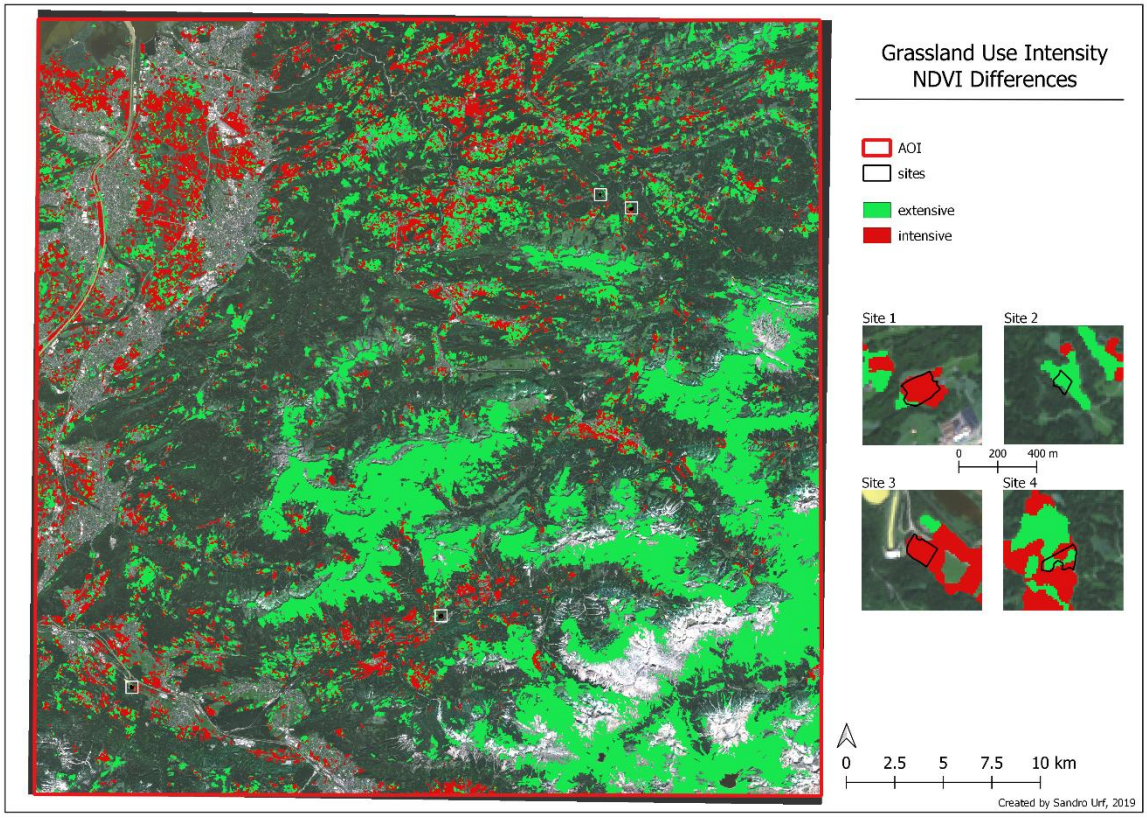

Figure 48: Grassland Use Intensity NDVI Differences.

NDVI min SD .25

Classification based on NDVImin mean with threshold standard deviation x .25 dropped to values of .54 and .14 regarding overall accuracy and Kappa. From the given 20.536 validations, 11.129 were assigned to the correct class. User´s accuracy reached .78 for extensive class and .38 for intensive classificated pixels. Values of producer´s accuracy achieved .46 and .72 for extensive respectively intensive classification (Table 17). The appendant map is shown in Figure 49.

Table 17: Accuracy Assessment NDVI min SD .25.

		Reference Data			
		Ext 0	**Int 1**	**sum**	**UA**
Classification	**Ext 0**	**6436**	1845	8281	0.78
	Int 1	7571	**4693**	12264	0.38
	sum	14007	6538	**11129**	-
	PA	0.46	0.72	-	-
				Overall	**0.54**
				Kappa	**0.14**

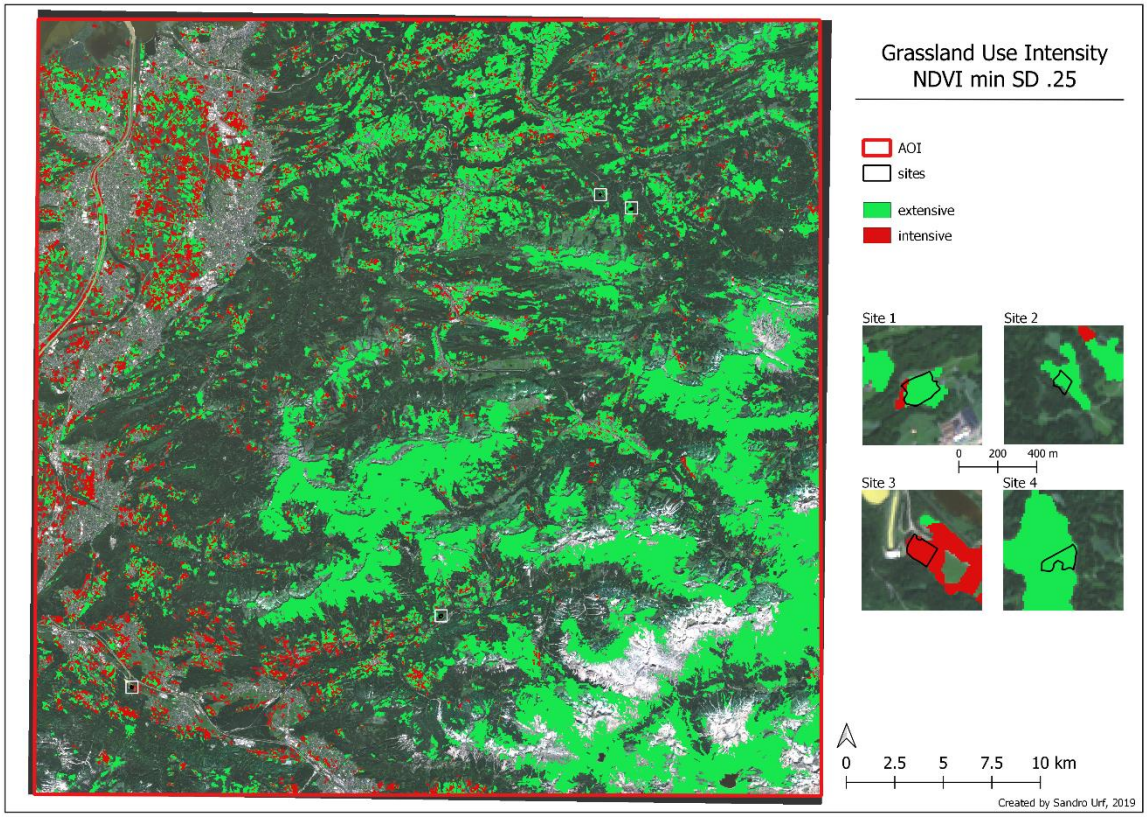

Figure 49: Grassland Use Intensity NDVImin SD .25.

NDVI min SD 1

In comparison, classification based on NDVImin mean with threshold standard deviation x1 dropped even more in terms of overall accuracy to .42 with Kappa .14. For extensive and intensive class, user´s accuracy achieved .99 respectively .03 and .41 respectively .79 regarding producer´s accuracy. From 20.536 validations, 8.530 were assigned to the corresponding correct class (Table 18). Figure 50 shows the corresponding map of the classification.

Table 18: Accuracy Assessment NDVI min SD 1.

		Reference Data			
		Ext 0	**Int 1**	**sum**	**UA**
Classification	**Ext 0**	**8193**	88	8281	0.99
	Int 1	11927	**337**	12264	0.03
	sum	20120	425	**8530**	-
	PA	0.41	0.79	-	-
				Overall	**0.42**
				Kappa	**0.14**

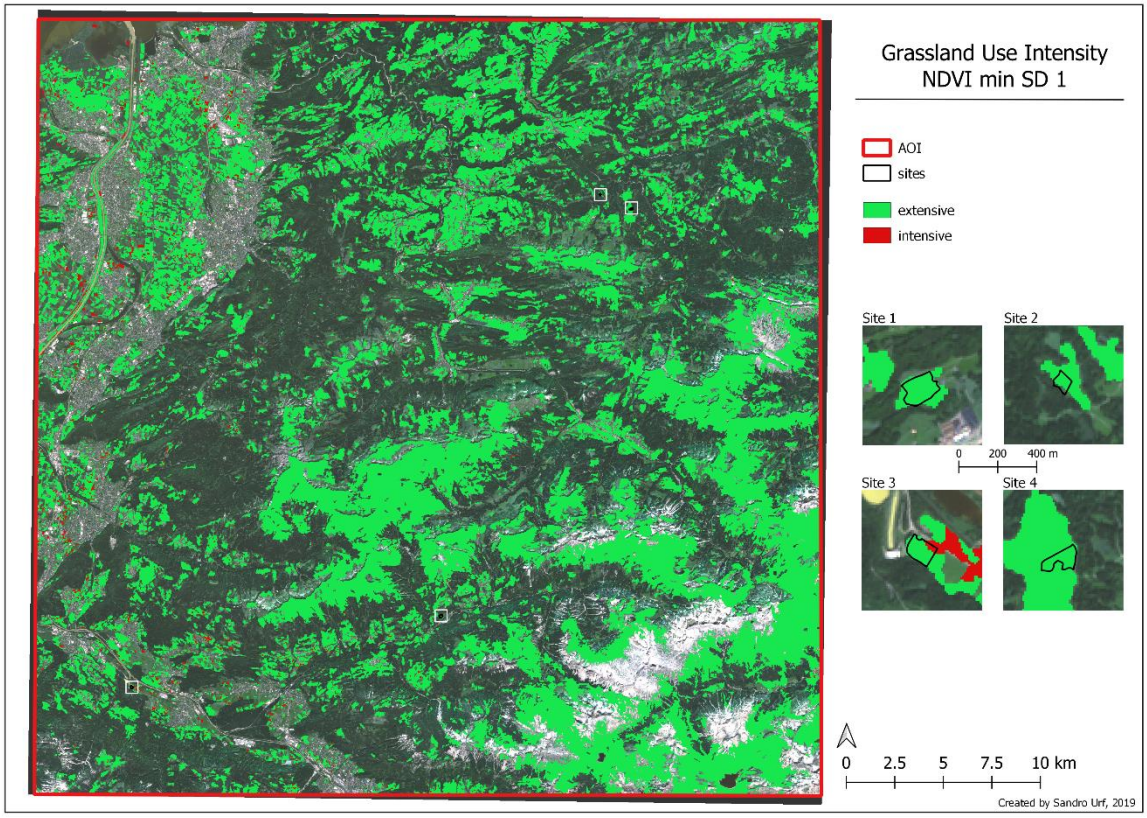

Figure 50: Grassland Use Intensity NDVImin SD 1.

8. Discussion

This chapter provides an examination of the results derived in chapter 7 including an in-depth analysis of the undertaken classifications. Along with an investigation of the individual sites and their classifications, the focus is also set on difficulties and problems occurred.

8.1. Land Cover Classification

Analysis of land cover classifications show different results depending on used sensors and chosen time spans. Overall conclusion is an improvement of results with increased number of sensors and timespans used – although, regarding class grassland, this statement does not apply (Table 8 to Table 12).

Sentinel-1 single sensor classification with time span over the whole year shows the least accurate result with overall accuracy of .69 and lowest Kappa .62. Inaccurate results are found especially in tree land cover classes broad leafed and conifer trees. As shown in 7.1, UA and PA reach from .49 to .56 with many mismatches between these classes. All other classes reach PA and UA > .62, where class 3 imperviousness shows lowest accuracies with most mismatches in classes 1 and 2, especially regarding producer´s accuracy. Water detection using RADAR-derived data with UA and PA of .98 and 1 is nearly excellent – one false assignment is given with class 2. Regarding accurate classification of classes 5 and 6, grassland and crop, time span of the whole year seems to be error biased. Most of the mismatches in these classes are assigned to the contrary class, although UA of grassland also shows >70 false classifications with classes 1 and 3.

Overall improvement in accuracy (OA, Kappa, PA and UA) is given with Sentinel-1 classification using data until June (Table 9). UA increased or stayed at same level for all given classes, PA also reached higher accuracy values in all classes except class 6, crop, with a drop of 12 percentage points. Biggest improvements are detected in tree land cover classes, especially conifer trees, with an addition of 36 percentage points in PA and 26 percentage points regarding UA. Best results are reached, as previous, for class water with fewer mismatches in general. Class grassland also reached an improvement compared to previous Sentinel-1 single sensor classification. Inaccuracies occur especially with class cropland, where approximately double as much mismatches occur compared to other classes.

Further improvement regarding accuracies is reached using Sentinel-2 optical data. Except class 1 (broad-leafed), PA and UA of no class dropped below .80. Regarding class grassland, with PA and UA .80 and .83, misclassifications occur especially with classes broad-leafed and cropland. Best accuracies are reached, besides class water with 1 UA and PA, in class imperviousness with given values .95 and .89 PA and UA.

The two best results are obtained with single sensor Sentinel-2 data including periods for the whole year and the first half of the year (Table 11), respectively multi sensor classification using optical and SAR data (Table 12). For both, OA and Kappa remain at same level, hence differences occur in PA and UA of individual classes with a maximum changes of +- 3 percentage points. For the thesis´ purpose, regarding grassland analysis, slightly better accuracies (PA: .84; UA: .85 vs. PA: .83; UA: .85) are achieved with Sentinel-2 single sensor classification. Analysis of feature influence

shows powerful impact of percentiles regarding the land cover classification, this occur especially for percentiles of features Brightness and NDVI (Table 19).

Table 19: Top 5 feature influence for best grassland classification.

Rank	Time Feature	Influence (%)
1	NDVI p025	7
2	Brightness p025	6
3	NDVI p010	5
-	Brightness p050	5
4	Brightness p075	4

8.2. Detection of Mowing Events

8.2.1. Vegetation Indices

As outlined by HALABUK et al. (2015) and NUMATA et al. (2007a), the NDVI is a feasible instrument regarding the detection of mowing frequency of grassland. Based on the NDVI, all investigated vegetation indices accomplish similar results to NDVI. All indices, namely GNDVI, IRECI, SAVI, EVI and EVI2, show very high correlation with NDVI within sites 1 to 4.

A crucial factor in detection of (healthy) vegetation and its mowing occurrence is the reflectance of wavelengths in the near-infrared region (NIR). Due various involved channels and their factors regarding particular indices (chapter 6.3), characteristics of value progression may differ, an appearance of a mowing event is reciprocated at all indices with a rapid drop of approx. 0.3 to 0.5, followed from a rise of distinct value. The rise of index values is directly linked to healthy vegetation´s chlorophyll content (HALABUK et al. 2015; NUMATA et al. 2007b; NUMATA et al. 2007a).

8.2.2. Interferometric Coherence

Results of coherence calculation and analysis of examined sites show a challenging interpretation regarding an explicit assertion and declaration of mowing events. In general, mowing activities can be detected, an increase of coherence values can be noticed, but due heterogeneity of calculated pixels, delimitations of the sites are not clearly comprehensible as shown in chapter 7.2.2, Figure 40 to Figure 45.

Change detection of grassland and vegetation in general using synthetic aperture radar data underlies, as pointed out by TAMM et al. (2016) and VOORMANSIK et al. (2013), multiple impacts such as diverging coherence results regarding chosen time of ingestion (ascending/descending orbit) due morning dew, farming activities, height and frequency of cuts, precipitation, wind conditions and types/species of grassland.

8.3. Grassland Use Intensity

Analysis of grassland use intensity shows different results for all used approaches, methods using SAR-coherence and NDVI differences/scene provide similar results though.

With the given methods, classifications with single polarization coherence VV and VH show nearly no differences regarding accuracy. For both classifications, producer´s accuracy for extensive and intensive class show values of .67 respectively .69. User´s accuracy on the other hand, show differences of 43 respectively 44 percent points between classes extensive and intensive with accuracies of .43 VV / .42 VH and .86 VV/VH leading to values below average accuracy (OA) regarding class extensive and above average accuracy values regarding class intensive (Table 14 and Table 15).

Similar results are provided with method using NDVI differences/scene showing overall accuracy of .65. Differences of UA and PA of classes extensive and intensive are more balanced but also indicate a wider range (UA 20pp; PA 9pp) compared to use intensity classification using coherence calculation. Regarding PA and UA, with values of .55 and .70 (extensive) respectively .75 and .61 (intensive), both classes show a shift assuming inconstancy of the chosen method (Table 16).

Methods using calculations of NDVI minima and its change per month using factors of standard deviation .25 and 1 achieved the least accurate results. Especially method using NDVImin SD 1 (Table 18) cannot be suggested due weak classification result of intensive usage and is further discussed in chapter 8.3.1.
A slightly better result is achieved with monthly change of NDVImin bigger than standard deviation .25. PA changed from .41 and .79 to .46 and .72 for classes extensive and intensive, whereas UA shift from .99 and .03 to .78 and .38 resulting in an increase of 12.7 percent points from 41,52% to 54,17% in terms of overall accuracy (Table 17).
As mentioned, methods using NDVI minima derived from monthly data achieved the most inaccurate results compared to classifications using coherence and NDVI differences per scene. Disadvantages using NDVI´s average minimum per month is the possibility of concealment given with potential rapid vegetation´s revitalization. This concealment-effect is amplified with decreasing number of available images – which restricts the advantages of optical satellite data in general. This occurs especially in regions with more distinct topographic characteristic. This can be, amongst others, lead back to increased occurrence of cloud formations resulting in non-applicable data.
The calculation of NDVI´s average minimum is with the given method not suitable. Further discussion takes place in the following chapter 8.3.1.

In general, classification approaches using coherence of polarizations VV and VH as well as NDVI differences per scene achieved Kappa values of around .30 (VV: .31; VH: .30; NDVIdiff: .30), while approaches using standard deviations of NDVI show low Kappa of .14.

8.3.1. Site Analysis

Following tables (Table 20 to Table 24) show a comparison of each classification per site. Although the sites have been assigned with an inwards-buffer of 10 metres, all sites reach into areas not classified as grassland – the least affected site of this inaccuracy is site 4.

Classification derived by coherence VV and VH (Table 20 and Table 21) illustrate, as the classification itself, broad similarities. Except site 2, all sites are classified with classes both, extensive and intensive. According to the used reference data, where a site is characterized by one designated class of usage, a multi-class classification within one site should not occur.
For both polarizations VV and VH, site 1 shows extensive classification in western and north-eastern part and intensive usage in the center. Regarding coherence VH classification, extensive classification in western area is smaller, whereas the eastern part is larger compared to classification performed with coherence VH.
In both classifications, site 2 is assigned to intensive used grassland. Site 3 and site 4 contain again, both extensive and intensive classified pixels. In both sites, extensive usage appears with larger areas using polarization VH compared to VV. According the statement of TAMM et al. (2016), an increase of coherence for VV polarization compared to VH polarization is detected with the used method and calculations.

Table 20: Site Analysis InCoherence VV.

Site 1	Site 2	Site 3	Site 4
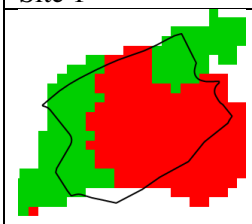	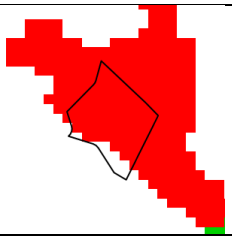	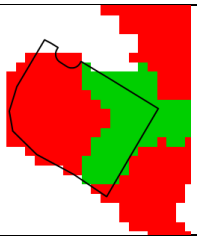	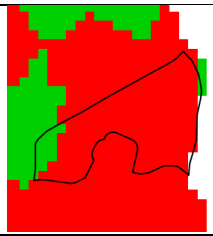

Table 21: Site Analysis InCoherence VH.

Site 1	Site 2	Site 3	Site 4
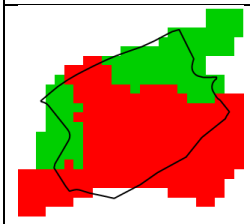	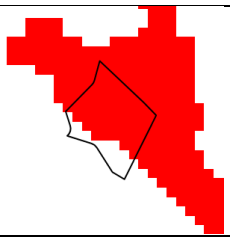	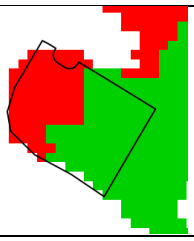	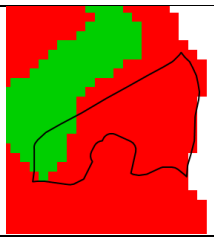

Site analysis of classifications derived by NDVI calculations (Table 22 to Table 24) show a more homogeneous result compared to coherence results (Table 20 and Table 21). Best NDVI classification result, respectively NDVIdiff per scene, shows occasionally inconstancies in the south-western area regarding site 1. Site 2 and site 3 present complete homogeneity within the sites, whereas site 4 shows the most heterogeneous outcome with no indication of prevalent use intensity (Table 22).

Table 22: Site Analysis NDVIdiff/scene.

Site 1	Site 2	Site 3	Site 4
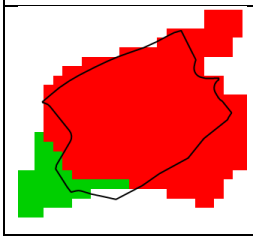	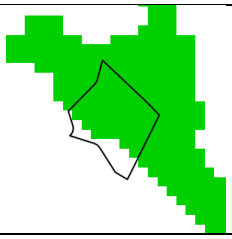	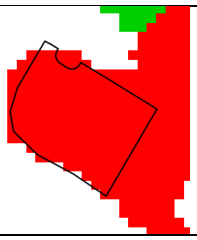	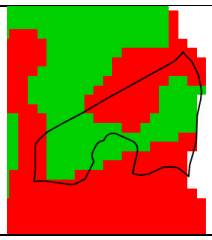

Classifications using change of monthly NDVImin with factors of calculated standard deviations, resulting in least accurate classifications, show the most homogeneous outcomes per site. Remarkable is the tendency to extensive classification result for both calculations, standard deviation .25 and 1 (Table 23 and Table 24). Differences occur especially regarding site 3, where a nearly complete change from intensive (Table 23) to extensive usage (Table 24) took place. Accuracies of this approaches in general, although lead to the tendency to assume approach using .25 standard deviation.

Table 23: Site Analysis NDVImin standard deviation .25.

Site 1	Site 2	Site 3	Site 4
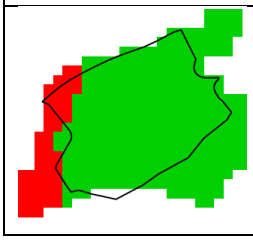	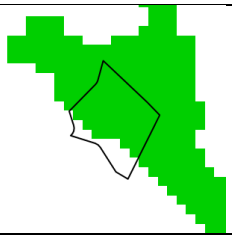	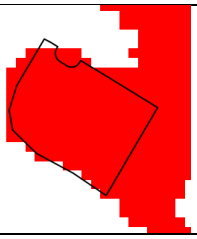	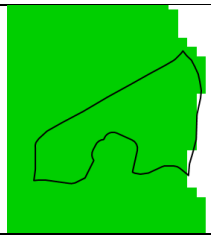

Table 24: Site Analysis NDVImin standard deviation 1.

Site 1	Site 2	Site 3	Site 4
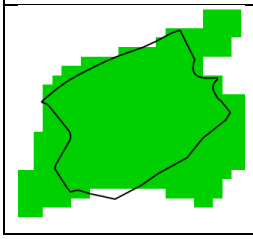	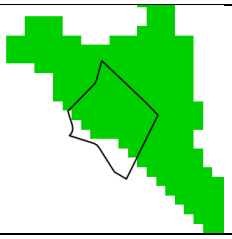	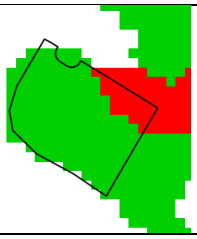	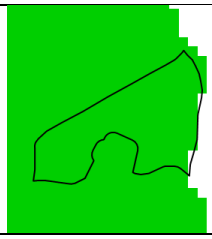

A comparison of each site for the different approaches shows a tendency of site 1 to be classified as intensive used grassland. This occurs for classifications with best accuracies, methods coherence and NDVI differences per scene. Whereas the coherence outcomes present a mix of extensive and intensive class, NDVI-approach is nearly complete classified as intensive. The fact of similar results for coherence and NDVI differences per scene is not given regarding site 2. All results show complete homogeneity within the site, although coherence products assign site 2 to class intensive and all NDVI-methods to class extensive. A possible reason for this outcome could be a poor availability of optical imagery due cloud coverage compared to SAR-data leading to information loss regarding mowing events.

Classifications of site 3 show various characteristics which are difficult to interpret. As mentioned, coherence classification shows heterogenous results with differences between polarizations VV and VH. Given the chosen method for accuracy assessment, which uses the polygon´s center for verification, site 3 shows different outcomes for each polarization. The two best NDVI-approaches show a complete classification as intensive used grassland for site 3, whereas tendency to extensive classification is given with method NDVI minimum and change of standard deviation 1.
Results for site 4 show a more conclusive outcome regarding coherence classifications. Despite mixed classifications within the site, majority is assigned to class intensive usage with exception of extensive classified areas at site´s western boundary. NDVI classifications show incongruent results with complete assignations to extensive class with NDVI minimum standard deviation methods and mixed classification without clear boundaries, meaning east/west or north/south delimitations, with approach using NDVI difference per scene.

8.3.2. Comparison of approaches and observed influences

Due to characteristics of SAR-sensors and their independence of atmospheric conditions (cloud occurrence, solar radiation, day/night), classifications could make use of higher image availability and therefore additional information supply compared to optical satellite data.
Linked to detection of mowing events (chapter 8.2) a heterogenous results within given sites (chapter 8.3.1) can be detected. This heterogeneousness in general and the deficiency of chosen approach using interferometric coherence is shown in Figure 51. Without altitude restriction of 1500m, as declared in the grassland use intensity definition (chapter 6.1), majority of classified pixels would change from extensive to intensive class, resulting in excessive absence of extensive class within entire AOI. Given this observation, a transfer to other regions, with and without exclusion of intensive grassland usage, should not be considered without adjustments of the model.
The height restriction of intensive used grassland to 1500m a.s.l. in general is a scheme fitted to European Alps and linked to given latitude and has to be adapted dynamically in dependency of given region.

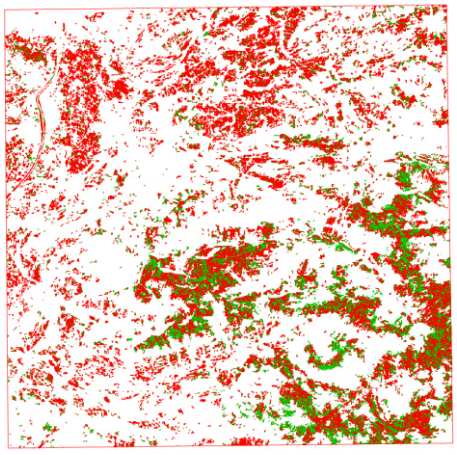

Figure 51: Grassland use intensity interferometric coherence VV – without height restriction.

Due to characteristics of optical sensor like Sentinel-2, a full image acquisition on regular basis is unusual, especially in topographic high distinctive regions with increased cloud formations like chosen area of interest. Cloud appearance in elevated and mountainous areas is given on a frequent basis, resulting in missing information regarding a potential grassland management scheme.
Referring to TAMM et al. (2016), with SAR-coherences a mowing event is detectable up to 24 days represented by high coherence values. This fact can not be observed with mowing occurrence detected with vegetation indices. Analysis of time series show a rapid rise of indices values after a mowing event resulting in high probability of missing a mowing occurrence with a possible given absence of imagery.
Another critical aspect regarding overestimating the frequency of mowing events is pointed out by KOLECKA et al. (2018). They reveal a similar effect happening to values of indices, in their study namely NDVI, like a mowing event or residues of clouds generated using fertilizers. After the application of fertilizer, NDVI shows a drop resulting in the necessity of previous knowledge about aspects of the farming management to counteract a low-grade accuracy and misinterpretations of classified data.

9. Conclusion

The aim of this thesis was to verify the suitability of optical and SAR-satellite-data regarding grassland mapping with an implemented differentiation of grassland use intensity in intensively and extensively used grassland. For this purpose, multiple approaches of two main categories have been conducted.
First approach used Sentinel-1 synthetic aperture radar data and its calculated interferometric coherence in polarizations VV and VH. Due to a bi-categoric classification, a SVM-classifier has been chosen. Second approach was carried out using NDVI-based classifications. Within NDVI-based classifications, attempts include the application of monthly mean NDVI minima and the usage of NDVI differences per Sentinel-2-scene.
Results show a similar outcome for classifications using computed coherences with polarizations VV and VH. Detailed site analysis can confirm this statement, where polarization VV could achieve slightly better results. In terms of accuracy, from NDVI approaches, the model using differences per scene accomplished best results.

i. does the combined use of optical and RADAR data add value in the classification of grassland compared to a single sensor classification?

Within this thesis, multiple classifications with various time spans, single and combined optical and RADAR data using Random Forest Classifier have been investigated. Regarding the classification of grassland, the best result could be achieved with Sentinel-2 single sensor data using time spans for full 2018 and first half of 2018. In comparison, grassland mapping with combined Sentinel-1 and Sentinel-2 data is negligible inferior. With given models, differences between these two classifications come up to one percent regarding producer´s accuracy and no change in user´s accuracy regarding class grassland.

ii. which, from optical sensors derived vegetation indices can be used to estimate mowing events?

The estimation and detection of mowing events with NDVI is undertaken in several studies, i.e. HALABUK et al. (2015); NESTOLA et al. (2016) (chapter 3). As discussed in chapter 6.3, in this research various indices have been calculated including NDVI, GNDVI, EVI, EVI2, IRECI and SAVI. Visual interpretations of indices show similar gradients for all examined vegetation indices. Result of visual interpretation could be verified with calculation of NDVI-based correlation coefficients. With examined sites, all indices show correlations .85 and above. Correlations below .90 only occur at site 3 with EVI and IRECI.
These high correlations between NDVI and other examined vegetation indices are indicating a suitability for all indices regarding the detection of grassland mowing events.

iii. Is the presented approach using Sentinel-1 SAR coherences suitable for detecting mowing events?

With the given approach and workflow, the detection of grassland mowing events using Sentinel-1 SAR coherences is feasible. Calculations show an increase of coherence values after the occurrence of a mowing event. Although, as discussed, various factors could affect the calculated values causing an inconstant development of coherence values. Also, an inconsistent distribution of coherence values can be detected within given sites resulting in a patchy site occurrence. The classification itself, as shown and discussed in chapter 7.3, 8.2.2 and 8.3, is suitable with limitations and under inclusion of altitude restrictions using a digital elevation model.

iv. which advantages/disadvantages using SAR coherences regarding grassland use intensity classifications compared to VI derived classifications can be detected?

With the tested approach using support vector machine classifier on SAR-coherence to map grassland use intensity, the result is suitable for conceived purpose after post processing and filtering. Results of the raw classification show a distinct speckle and inconsistence assignation to intensive and extensive class. With applied classification excluding post processing, an unmistakable assignment of a site (reference polygon) to one of the two classes cannot be ensured. An additional consideration of LOIs topographic characteristics increases the accuracy, although the result is not tenable. The combination of post processing and exclusion of class 'intensive' by altitude gives a meaningful base for further classification development.
Although SAR-data ensures a consistent and periodically image acquisition compared to optical derived classification, the results are similar for both approaches. Weakness of both classifications can be detected regarding class 'extensive' with low producer´s accuracy at NDVI-derived-, and low user´s accuracy at coherence-derived approach resulting in overall accuracies below 70%.

As shown in this thesis, given a powerful and stable satellite-based method for estimation of grassland use intensity, besides the sustainable availability of satellite data, especially knowledge of topographic, seasonal and predominant farming scheme aspects seem to be crucial in consideration of an accurate classification and interpretation of accomplished results.
All tested vegetation indices within this thesis seem to be practicable to detect mowing events. Further research regarding optical vegetation indices could include additional indices like S2REP (Sentinel-2 Red Edge Position), LCI (Leaf Chlorophyll Index) and LAI (Leaf Area Index).
In consideration of use intensity classification´s enhancement, a classification including the combination of optical and SAR-satellite data is conceivable. This would compensate the disadvantage

of optical data, like reliance on clear weather conditions or daylight, and include powerful radar information of SAR-sensors.

For further research, more attention could be paid to topographic characteristics of given area. Additional information acquired with calculations of the digital elevation model, e.g. slope and its linkage to the possibility of intensive grassland usage, can be considered. Furthermore, additional data regarding precipitation could be reconsidered to estimate its accurate influence referring to coherence values.

References

ALBERTZ, J. and M. WIGGENHAGEN (2009): Taschenbuch zur Photogrammetrie und Fernerkundung: Guide for photogrammetry and remote sensing. Heidelberg.

ALI, I., F. CAWKWELL, E. DWYER, B. BARRETT and S. GREEN (2016): Satellite remote sensing of grasslands: from observation to management. In: Journal of Plant Ecology 9 (6): 649–671.

AL-OBAIDEY, E. and S. AL-BALDAWI (2019): The study of NDVI fluctuation in southern Iraq(Hor Ibn Najim) using remote sensing data. In: Al-Mustansiriyah Journal of Science 30 (1): 1–6.

AREKHI, M., C. GOKSEL, F. BALIK SANLI and G. SENEL (2019): Comparative Evaluation of the Spectral and Spatial Consistency of Sentinel-2 and Landsat-8 OLI Data for Igneada Longos Forest. In: ISPRS International Journal of Geo-Information 8 (2): 56.

ARORA, M. K. (2010): Land cover classification from Remote Sensing data. Geospatial World. internet: https://www.geospatialworld.net/article/land-cover-classification-from-remote-sensing-data/ (12/08/2019).

BALLIN, M., G. BARCAROLI, M. MASSELLI and M. SCARNÓ (2018): Redesign sample for Land Use/Cover Area frame Survey (LUCAS) 2018: 56.

BEKKEMA, M. E. and M. ELEVELD (2018): Mapping Grassland Management Intensity Using Sentinel-2 Satellite Data. In: GI_Forum 1: 194–213.

BELGIU, M. and L. DRĂGUŢ (2016): Random forest in remote sensing: A review of applications and future directions. In: ISPRS Journal of Photogrammetry and Remote Sensing 114: 24–31.

CALLA, O. P. N. (1990): Applications of Microwave Remote Sensing. In: Indian Journal of Radio & Space Physics 19: 343–358.

CANDIAGO, S., F. REMONDINO, M. DE GIGLIO, M. DUBBINI and M. GATTELLI (2015): Evaluating Multispectral Images and Vegetation Indices for Precision Farming Applications from UAV Images. In: Remote Sensing 7 (4): 4026–4047.

CCRS, C. C. for R. S. (n.d.): Fundamentals of Remote Sensing. internet: https://www.nrcan.gc.ca/sites/www.nrcan.gc.ca/files/earthsciences/pdf/resource/tutor/fundam/pdf/fundamentals_e.pdf (02/10/2020).

CLERICI, N., C. A. VALBUENA CALDERÓN and J. M. POSADA (2017): Fusion of Sentinel-1A and Sentinel-2A data for land cover mapping: a case study in the lower Magdalena region, Colombia. In: Journal of Maps 13 (2): 718–726.

CONGALTON, R. G. (1991): A review of assessing the accuracy of classifications of remotely sensed data. In: Remote Sensing of Environment 37 (1): 35–46.

CRACKNELL, A. P. (2018): The development of remote sensing in the last 40 years. In: International Journal of Remote Sensing 39 (23): 8387–8427.

DENIZE, J., L. HUBERT-MOY, J. BETBEDER, S. CORGNE, J. BAUDRY and E. POTTIER (2018): Evaluation of Using Sentinel-1 and -2 Time-Series to Identify Winter Land Use in Agricultural Landscapes. In: Remote Sensing 11 (1): 37.

DLR, D. Z. fuer L. R. e. V. (2020): ECoLaSS. ecolass. internet: https://www.ecolass.eu/project-partners (05/05/2020).

DOGAN, C. and Y. BOZKURT (2017): Determination of Grassland Areas by Using Remote Sensing and Geographic Information Systems, with Special Reference to Isparta, Turkey. In: Scientific Papers: Series D, Animal Science - The International Session of Scientific Communications of the Faculty of Animal Science 60: 221–225.

DUSSEUX, P., T. CORPETTI, L. HUBERT-MOY and S. CORGNE (2014): Combined Use of Multi-Temporal Optical and Radar Satellite Images for Grassland Monitoring. In: Remote Sensing 6 (7): 6163–6182.

ESTEL, S., S. MADER, C. LEVERS, P. H. VERBURG, M. BAUMANN and T. KUEMMERLE (2018): Combining satellite data and agricultural statistics to map grassland management intensity in Europe. In: Environmental Research Letters 13 (7): 074020.

EUROPEAN COMMISSION (2019): Evolution of Copernicus Land Services based on Sentinel data | ECoLaSS Project | H2020. CORDIS | European Commission. internet: https://cordis.europa.eu/project/id/730008 (05/05/2020).

EUROPEAN COMMISSION (2016): Copernicus - The European Earth Observation Programme. Text. Internal Market, Industry, Entrepreneurship and SMEs - European Commission. internet: https://ec.europa.eu/growth/sectors/space/copernicus_en (12/01/2019).

EUROPEAN COMMISSION (2013): Interpretation Manual of European Union Habitats - EUR28. internet: http://ec.europa.eu/environment/nature/legislation/habitatsdirective/docs/Int_Manual_EU28.pdf (01/27/2019).

EUROPEAN PARLIAMENT (2013): Regulation (EU) No 1306/2013 of the European Parliament and of the Council of 17 December 2013 on the financing, management and monitoring of the common agricultural policy and repealing Council Regulations (EEC) No 352/78, (EC) No 165/94, (EC) No 2799/98, (EC) No 814/2000, (EC) No 1290/2005 and (EC) No 485/2008: 59.

EUROPEAN SPACE AGENCY ESA (2000a): User Guides - Sentinel-1 SAR - Level-1 - Sentinel Online. internet: https://sentinel.esa.int/web/sentinel/user-guides/sentinel-1-sar/product-types-processing-levels/level-1 (04/19/2020).

EUROPEAN SPACE AGENCY ESA (2000b): User Guides - Sentinel-1 SAR - Interferometry - Sentinel Online. internet: https://sentinel.esa.int/web/sentinel/user-guides/sentinel-1-sar/product-overview/interferometry (04/18/2020).

EUROPEAN SPACE AGENCY ESA (2000c): Missions - Sentinel Online. internet: https://sentinel.esa.int/web/sentinel/missions (12/01/2019).

EUROPEAN SPACE AGENCY ESA (2000d): Heritage - Sentinel-5 - Sentinel Online. internet: https://sentinel.esa.int/web/sentinel/missions/sentinel-5/overview/heritage (12/01/2019).

EUROPEAN SPACE AGENCY ESA (2000e): Applications. Overview. internet: http://www.esa.int/Applications/Observing_the_Earth/Copernicus/Overview4 (12/01/2019).

EUROPEAN SPACE AGENCY ESA (2000f): User Guides - Sentinel-1 SAR - Acquisition Modes - Sentinel Online. internet: https://sentinel.esa.int/web/sentinel/user-guides/sentinel-1-sar/acquisition-modes (02/22/2020).

EUROPEAN SPACE AGENCY ESA (2000g): MSI Instrument – Sentinel-2 MSI Technical Guide. internet: https://sentinel.esa.int/web/sentinel/technical-guides/sentinel-2-msi/msi-instrument (02/11/2020).

EUROPEAN SPACE AGENCY ESA (2000h): User Guides - Sentinel-2 MSI - Sentinel Online. internet: https://sentinel.esa.int/web/sentinel/user-guides/sentinel-2-msi (02/12/2020).

EUROPEAN SPACE AGENCY ESA (2000i): Radiometric - Resolutions - Sentinel-2 MSI - User Guides - Sentinel Online. internet: https://sentinel.esa.int/web/sentinel/user-guides/sentinel-2-msi/resolutions/radiometric (02/22/2020).

EUROPEAN UNION (2017): LUCAS - The EU´s Land Use and Land Cover Survey. internet: https://ec.europa.eu/eurostat/documents/4031688/8503684/KS-01-17-069-EN-N.pdf/91e45d7a-ee8c-47ea-a666-f49600d1ee6c (10/27/2019).

EUROPEAN UNION (1995): Integrated Administration and Control System (IACS). Text. European Commission - European Commission. internet: https://ec.europa.eu/info/food-farming-fisheries/key-policies/common-agricultural-policy/income-support/controls-and-transparency/managing-payments_en (10/13/2019).

FARAMARZI, M., Z. HEIDARIZADI, A. MOHAMADI and M. HEYDARI (2018): Detection of Vegetation Changes in Relation to Normalized Difference Vegetation Index (NDVI) in Semi-Arid Rangeland in Western Iran. In:)NDVI(بررسی تغییرات پوشش گیاهی در ارتباط با شاخص تفاضل پوشش گیاهی در مراتع نیمه خشک غرب ایران 20 (1): 51–60.

FRAMPTON, W. J., J. DASH, G. WATMOUGH and E. J. MILTON (2013): Evaluating the capabilities of Sentinel-2 for quantitative estimation of biophysical variables in vegetation. In: ISPRS Journal of Photogrammetry and Remote Sensing 82: 83–92.

FRANKE, J., V. KEUCK and F. SIEGERT (2012): Assessment of grassland use intensity by remote sensing to support conservation schemes. In: Journal for Nature Conservation 20 (3): 125–134.

GAF AG (2018): D33.1a – Time Series Analysis for Thematic Classification (Issue 1). internet: https://docs.wixstatic.com/ugd/c90769_ec290c1429144bb082a1254fb2c22024.pdf (01/27/2019).

GISLASON, P. O., J. A. BENEDIKTSSON and J. R. SVEINSSON (2006): Random Forests for land cover classification. In: Pattern Recognition Letters 27 (4): 294–300.

GITELSON, A. A., Y. J. KAUFMAN and M. N. MERZLYAK (1996): Use of a green channel in remote sensing of global vegetation from EOS-MODIS. In: Remote Sensing of Environment 58 (3): 289–298.

GÓMEZ GIMÉNEZ, M., R. DE JONG, R. DELLA PERUTA, A. KELLER and M. E. SCHAEPMAN (2017): Determination of grassland use intensity based on multi-temporal remote sensing data and ecological indicators. In: Remote Sensing of Environment 198: 126–139.

HALABUK, A., M. MOJSES, M. HALABUK and S. DAVID (2015): Towards Detection of Cutting in Hay Meadows by Using of NDVI and EVI Time Series. In: Remote Sensing 7 (5): 6107–6132.

HONG, G., A. ZHANG, F. ZHOU and B. BRISCO (2014): Integration of optical and synthetic aperture radar (SAR) images to differentiate grassland and alfalfa in Prairie area. In: International Journal of Applied Earth Observation and Geoinformation 28: 12–19.

HUETE, A., C. JUSTICE and W. VAN LEEUWEN (1999): MODIS Vegation Index. Algorithm Theoretical Basis Document: 129.

HUETE, A. R. (1988): A soil-adjusted vegetation index (SAVI). In: Remote Sensing of Environment 25 (3): 295–309.

ISSELSTEIN, J., DEUTSCHE AGRARFORSCHUNGSALLIANZ, T. MICHAELIS and G. BELLOF (2015): The Grassland Expert Forum: innovative use of grassland for resource protection: the DAFA research strategy. Braunschweig.

JIANG, Z., A. HUETE, K. DIDAN and T. MIURA (2008): Development of a two-band enhanced vegetation index without a blue band. In: Remote Sensing of Environment 112: 3833–3845.

JOANNEUM RESEARCH (2019): D43.1b-Prototype Report: Improved Permanent Grassland. internet: https://6c1e2b9b-e840-4757-9a09-97d14ddbfe72.filesusr.com/ugd/c90769_a42e2f1d9abc490f92ff1f137726e1e9.pdf (05/05/2020).

KEUCK, V., J. FRANKE and F. SIEGERT (2010): Remote sensing-based products for biomass assessment in Europa. Brussels.

KHORRAM, S., C. F. van der WIELE, F. H. KOCH, S. A. C. NELSON and M. D. POTTS (2016): Principles of applied remote sensing. Cham Heidelberg New York.

KOLECKA, N., C. GINZLER, R. PAZUR, B. PRICE and P. VERBURG (2018): Regional Scale Mapping of Grassland Mowing Frequency with Sentinel-2 Time Series. In: Remote Sensing 10 (8): 1221.

KÖPPEN, W. (1936): Das geographische System der Klimate. 1: 44.

KOTTEK, M., J. GRIESER, C. BECK, B. RUDOLF and F. RUBEL (2006): World Map of the Köppen-Geiger climate classification updated. In: Meteorologische Zeitschrift 15 (3): 259–263.

KULKARNI, A. D. and B. LOWE (2016): Random Forest Algorithm for Land Cover Classification. In: International Journal on Recent and Innovation Trends in Computing and Communication 4 (3): 7.

LANDIS, J. R. and G. G. KOCH (1977): The Measurement of Observer Agreement for Categorical Data. In: Biometrics 33 (1): 159.

LATHAM, J. S. and R. CUMANI (2014): Global Land Cover SHARE (GLC-SHARE): 40.

LEVIN, N. (1999): Fundamentals of Remote Sensing: 225.

LILLESAND, T., R. W. KIEFER and J. CHIPMAN (^{6}2008): Remote Sensing and Image Interpretation.

MOREIRA, A., P. PRATS-IRAOLA, M. YOUNIS, G. KRIEGER, I. HAJNSEK and K. P. PAPATHANASSIOU (2013): A tutorial on synthetic aperture radar. In: IEEE Geoscience and Remote Sensing Magazine 1 (1): 6–43.

MOUNTRAKIS, G., J. IM and C. OGOLE (2011): Support vector machines in remote sensing: A review. In: ISPRS Journal of Photogrammetry and Remote Sensing 66 (3): 247–259.

NAN, Z. B. (2001): REMOTE SENSING APPLICATION TO GRASSLAND MONITORING. In: (2001).

NASA (n.d.): MODIS Web. internet: https://modis.gsfc.nasa.gov/about/ (08/31/2019).

NESTOLA, E., C. CALFAPIETRA, C. A. EMMERTON, C. Y. S. WONG, D. R. THAYER and J. A. GAMON (2016): Monitoring Grassland Seasonal Carbon Dynamics, by Integrating MODIS NDVI, Proximal Optical Sampling, and Eddy Covariance Measurements. In: Remote Sensing 8 (3): 260.

NICULESCU, S., C. LARDEUX and J. HANGANU (2018a): Synergy between Sentinel-1 radar time series and Sentinel-2 optical for the mapping of restored areas in Danube delta. In: Proceedings of the ICA 1: 1–10.

NICULESCU, S., H. TALAB OU ALI and A. BILLEY (2018b): Random forest classification using Sentinel-1 and Sentinel-2 series for vegetation monitoring in the Pays de Brest (France). In: NEALE, C. M. and A. MALTESE (eds.) (2018b): Remote Sensing for Agriculture, Ecosystems, and Hydrology XX. Berlin, Germany: 6. internet: https://www.spiedigitallibrary.org/conference-proceedings-of-spie/10783/2325546/Random-forest-classification-using-Sentinel-1-and-Sentinel-2-series/10.1117/12.2325546.full (09/02/2019).

NUMATA, I., D. A. ROBERTS, O. A. CHADWICK, J. SCHIMEL, F. R. SAMPAIO, F. C. LEONIDAS and J. V. SOARES (2007a): Characterization of pasture biophysical properties and the impact of grazing intensity using remotely sensed data. In: Remote Sensing of Environment 109 (3): 314–327.

NUMATA, I., D. A. ROBERTS, Y. SAWADA, O. A. CHADWICK, J. P. SCHIMEL and J. V. SOARES (2007b): Regional Characterization of Pasture Changes through Time and Space in Rondônia, Brazil. In: Earth Interactions 11 (14): 1–25.

NWS, N. W. S. (n.d.): NWS JetStream MAX - Addition Köppen Climate Subdivisions. internet: https://web.archive.org/web/20181224025419/https://www.weather.gov/jetstream/climate_max (09/22/2019).

PAL, M. (2003): Random forests for land cover classification. In: (2003): IGARSS 2003. 2003 IEEE International Geoscience and Remote Sensing Symposium. Proceedings (IEEE Cat. No.03CH37477), volume 6. Toulouse, France: 3510–3512. internet: http://ieeexplore.ieee.org/document/1294837/ (01/28/2019).

ROUSE, W. and R. H. HAAS (1974): MONITORING VEGETATION SYSTEMS IN THE GREAT PLAINS WITH ERTS: 9.

RUBEL, F., K. BRUGGER, K. HASLINGER and I. AUER (2017): The climate of the European Alps: Shift of very high resolution Köppen-Geiger climate zones 1800–2100. In: Meteorologische Zeitschrift 26 (2): 115–125.

SAKOWSKA, K., R. JUSZCZAK and D. GIANELLE (2016): Remote Sensing of Grassland Biophysical Parameters in the Context of the Sentinel-2 Satellite Mission. In: Journal of Sensors 2016: 1–16.

SCHIRPKE, U., M. KOHLER, G. LEITINGER, V. FONTANA, E. TASSER and U. TAPPEINER (2017): Future impacts of changing land-use and climate on ecosystem services of mountain grassland and their resilience. In: Ecosystem Services 26: 79–94.

SCURLOCK, J. M. O. and D. O. HALL (1998): The global carbon sink: a grassland perspective. In: Global Change Biology 4 (2): 229–233.

STENZEL, S., F. E. FASSNACHT, B. MACK and S. SCHMIDTLEIN (2017): Identification of high nature value grassland with remote sensing and minimal field data. In: Ecological Indicators 74: 28–38.

STORY, M. and R. CONGALTON (1986): Accuracy Assessment: A User's Perspective: 3.

TAMM, T., K. ZALITE, K. VOORMANSIK and L. TALGRE (2016): Relating Sentinel-1 Interferometric Coherence to Mowing Events on Grasslands. In: Remote Sensing 8 (10): 802.

TSO, B. and P. M. MATHER (2009): Classification methods for remotely sensed data. Environmental engineering. Boca Raton, Fla. London New York.

TUELLER, P. T. (1989): Remote sensing technology applications. In: JOURNAL OF RANGE MANAGEMENT: 12.

VOORMANSIK, K., T. JAGDHUBER, A. OLESK, I. HAJNSEK and K. P. PAPATHANASSIOU (2013): Towards a detection of grassland cutting practices with dual polarimetric TerraSAR-X data. In: International Journal of Remote Sensing 34 (22): 8081–8103.

VOORMANSIK, K., T. JAGDHUBER, K. ZALITE, M. NOORMA and I. HAJNSEK (2016): Observations of Cutting Practices in Agricultural Grasslands Using Polarimetric SAR. In: IEEE Journal of Selected Topics in Applied Earth Observations and Remote Sensing 9 (4): 1382–1396.

WOLFF, C. (n.d.): Radar Basics - Synthetic Aperture Radar. internet: https://www.radartutorial.eu/20.airborne/ab07.en.html (02/23/2020).

XU, L., H. ZHANG, C. WANG, B. ZHANG and M. LIU (2018): Crop Classification Based on Temporal Information Using Sentinel-1 SAR Time-Series Data. In: Remote Sensing 11 (1): 53.